Andreas Katzensteiner, BSc

UNIAXIAL TENSILE, RUPTURE AND EXTENSION-INFLATION TESTS ON OVINE ESOPHAGI

MASTER THESIS

For obtaining the academic degree
Diplom-Ingenieur

Master Programme of
Technical Physics

Graz University of Technology

Supervisor:
Professor Laurentius Windholz
Institute of Experimental Physics
in cooperation with
Institute of Biomechanics

Graz, December 7, 2011

Contents

Abstract

Congenital defects of the esophagus are quite frequent. A new method of treatment by implanting tissue engineered esophagi into newborns is currently being developed and tested on ovine esophagi, yet the biomechanical behavior of ovine esophagus is still not understood very well. The aim of this work is to increase the knowledge of the mechanical response of ovine esophagus to uniaxial stretching and extension-inflation to help improving tissue-engineered esophagi. Therefore, twelve esophagi of slaughtered lambs were mechanically investigated. For the tensile and rupture tests, they were separated into their distinctive layers (mucosa-submucosa and muscle), and prepared as strip samples oriented along the axial and circumferential direction. For the extension-inflation tests the esophagi were prepared as tube samples. The passive uniaxial mechanical response and the rupture strength of the prepared strip samples were investigated in a $37\,^{\circ}\mathrm{C}$ physiological saline under quasistatic loading conditions to determine the stress-stretch behavior in the axial and circumferential direction. The pressure-stretch behavior of the prepared tube samples were investigated through inflating the tube with a $37\,^{\circ}\mathrm{C}$ physiological saline. The obtained stress-stretch diagramms from the tensile and rupture tests and the pressure-stretch diagramms from the extension-inflation tests were evaluated and can be used for future analysis, e.g., for constitutive modeling and for finite element simulations. The results show, that the muscle was stiffer in axial direction, but softer in circumferential direction than the respective directions of the mucosa-submucosa. The mucosa-submucosa was also stiffer in axial than in circumferential direction. The rupture strength of the mucosa-submucosa was much higher than the rupture strength of the muscle. Both layers had a higher rupture strength in axial direction. The extension-inflation tests showed a strong softening of the esophagi in circumferential direction. In conclusion, the ovine esophagus showed a heterogenous, anisotropic behavior, with different mechanical properties in the individual layers as well as depending on the orientation of the measurement. These mechanical responses of the investigated tissue could be used as a benchmark for improving tissue engineered esophagi.

Aufgabenstellung

Angeborene Defekte der Speiseröhre sind recht häufig. Eine neue Behandlungsmethode, bei der tissue-engineerte Speiseröhren in Neugeborene eingesetzt werden, wird zur Zeit entwickelt und an Lammspeiseröhren getestet. Das biomechanische Verhalten von Lammspeiseröhren ist aber immer noch wenig erforscht. Das Ziel dieser Arbeit ist das Wissen über die mechanische Reaktion von Lammspeiseröhren auf uniaxiale Dehnung und Druckdehnung zu erweitern, um bei der Verbesserung von tissue-engineerten Speiseröhren zu helfen. Zu diesem Zweck wurden zwölf Speiseröhren von geschlachteten Lämmern mechanisch untersucht. Diese wurden für die Dehnungs- und Bruchtests in ihre einzelnen Schichten (Mucosa-Submucosa und Muskelschicht) zerlegt, und als Streifenproben, orientiert in Axial- und Umfangsrichtung, präpariert. Für die Druck-Dehnungstests wurden die Speiseröhren als schlauchförmige Proben präpariert. Die passiven uniaxialen mechanischen Reaktionen und die Reissfestigkeit der vorbereiteten Streifenproben wurden in einer $37\,^{\circ}\mathrm{C}$ physiologischen Salzlösung unter quasistatischen (fast statischen) Belastungsbedingungen untersucht, um das Spannungs-Dehnungsverhalten in Axial- und Umfangsrichtung zu bestimmen. Das Druck-Dehnungsverhalten der vorbereiteten schlauchförmigen Proben wurde durch aufblasen der Röhren mit einer $37\,^{\circ}\mathrm{C}$ physiologischen Salzlösung erforscht. Die aus den Dehnungs- und Bruchtests gewonnenen Spannungs-Dehnungsdiagramme sowie die aus den Inflationstests gewonnenen Druck-Dehnungsdiagramme wurden ausgewertet und können für zukünftige Analysen, wie z.B. für konstitutive Modellierungen und für Finite Elemente Simulationen, verwendet werden. Die Resultate zeigen, dass der Muskel in Axialrichtung steifer, in Umfangsrichtung aber weicher als die jeweiligen Orientierungen der Mucosa-Submucosa war. Auch die Mucosa-Submucosa war in Axialrichtung steifer als in Umfangsrichtung. Die Reissfestigkeit der Mucosa-Submucosa war wesentlich höher als die Reissfestigkeit des Muskels. Beide Schichten zeigten eine höhere Reissfestigkeit in Axialrichtung. Die Druckdehnungstests zeigten eine starke Erweichung der Speiseröhren in Umfangsrichtung. Insgesamt zeigte die Lammspeiseröhre ein heterogenes, anisotropisches Verhalten mit unterschiedlichen mechanischen Eigenschaften sowohl in den einzelnen Schichten als auch abhängig von den Orientierungen der Messungen. Diese mechanischen Reaktionen des untersuchten Gewebes können als Massstab zur Verbesserung tissue-engineerter Speiseröhren verwendet werden.

Acknowledgment

I acknowledge the excellent supervision of Univ.-Prof. Dipl.-Ing. Dr. techn. Gerhard A. HOLZAPFEL and Univ.-Prof. Dipl.-Ing. Dr. techn. Laurentius WINDHOLZ.

I especially acknowledge the proactively guidance and support of my co-advisors Dipl. Ing. Dr. techn. Gerhard SOMMER und Dipl. Ing. Andreas J. SCHRIEFL.

Furthermore, I want to thank Herwig AINÖDHOFER for providing the samples, as well as Manuel HUBER and Martin KERN for introducing me to the testing machine.

1 Introduction

1.1 What is biomechanics?

The term Biomechanics consists of two words: biology and mechanics, which suggests, that biomechanics investigates the mechanical behavior of biological systems. That is almost exactly what Jay D. Humphrey wrote in his book *Cardiovascular Solid Mechanics: Cells, Tissues, and Organs* (Humphrey, 2002):

> *'Biomechanics can be defined as the development, extension, and application of mechanics to answer questions of importance in biology and medicine. It is only through biomechanics that we can understand, an thus address, many of the biophysical phenomena that occur at the molecular, cellular, tissue, organ, and organism levels. Hence, biomechanics is as important as it is challenging'*

In biomechanics, the unterstanding of the basic relations between stress and strain is very important. In contradiction to the behavior of most materials, where stress and strain are related linearly via Young's modulus, biological tissues show a much more complicated mechanical behavior due to heterogenous, anisotropic and viscoelastic properties. So if we want to know, how living systems like the human circulatory system or the gastrointestinal systems of sheeps, work, we have to use biomechanical methods to understand their behavior, which requires understanding of mathemathics, mechanics, statistics, and biology (Gregersen, 2003).

1.2 Historical development

The history of biomechanics begins in ancient greece with the book *On the Parts of Animals* by Aristotle (384-322 B.C.), where he described the anatomy and function of the internal organs, especially an accurate description of the peristaltic motion of the ureter. The further development of biomechanics is strongly correlated with the development of mechanics and engineering. Remarkable contributors to biomechanics were:

Santorio Santorio (1561-1636), who laid the foundation of the modern study of metabolism;

Galileo Galilei (1564-1642), who used the constant period of a pendulum to measure the pulse rate of people and designed one of the first microscopes;

William Harvey (1578-1658), who discovered the blood circulation in 1615;

Giovanni Alfonso Borelli (1608-1679), who wrote the book *On Motion of Animals* in 1680 and investigated the flight of birds and the swimming of fish, as well as the movements of the heart and of the intestines;

Isaac Newton (1642-1727), whos laws of motion and constitutive equations are the foundation of biomechanics;

Thomas Young (1773-1829), who developed Youngs' modulus and identified the formation of the human voice as vibrations of elastic materials;

Herrmann von Helmholtz (1821-1894), whos contributions to biomechanics give him the title 'Father of Bioengineering';

and many others like Adolf Fick (1829-1901), Diederick Johannes Korteweg (1848-1941), Horace Lamb (1849-1934), Otto Frank (1865-1944) and Balthasar van der Pol (1889-1959) (Fung, 1993).

The studies of biomechanics in the 20th century were mostly concentrated on the cardiovascular field and orthopaedics, not on gastroenterology, but there were also some few, who investigated the gastrointestinal tract. Walter B. Cannons book *The mechanical Factors of Digestion* is here to be mentioned, as well as the research groups of Fung, Brasseur, Miftakhov and Gregersen (Gregersen, 2003).

1.3 Motivation

This master's thesis is part of a project of the Institute of Biomechanics of the University of Technology and the Pediatric Department of the Medical University in Graz. The goal is to understand the biomechanical behavior of ovine esophagi and to compare it with the behavior of tissue engineered esophagi. The tissue engineering group of the Pediatric Department under the leadership of Professor Amulya Saxena M.D. is developing a method to implant tissue engineered esophagi into newborns with esophageal atresia.
Esophageal atresia is defined as following:

> *'Esophageal atresia (EA) is a developmental defect of the upper gastrointestinal tract in which the continuity between the upper and lower esophagus is lost. EA can occur with or without tracheoesophageal fistula (TEF), an abnormal connection between the trachea and the esophagus.' (Scott, 2009)*

Esophageal atresia occurs in one of 3000 to 5000 births. It can occur in many anatomic variations: The most common with a percentage of 87 % is a blind esophageal pouch with a fistula between the trachea and the lower half of the esophagus. Other forms like an isolated atresia or an isolated TEF occur less often (Fig. 1.1) (Clark, 1999).

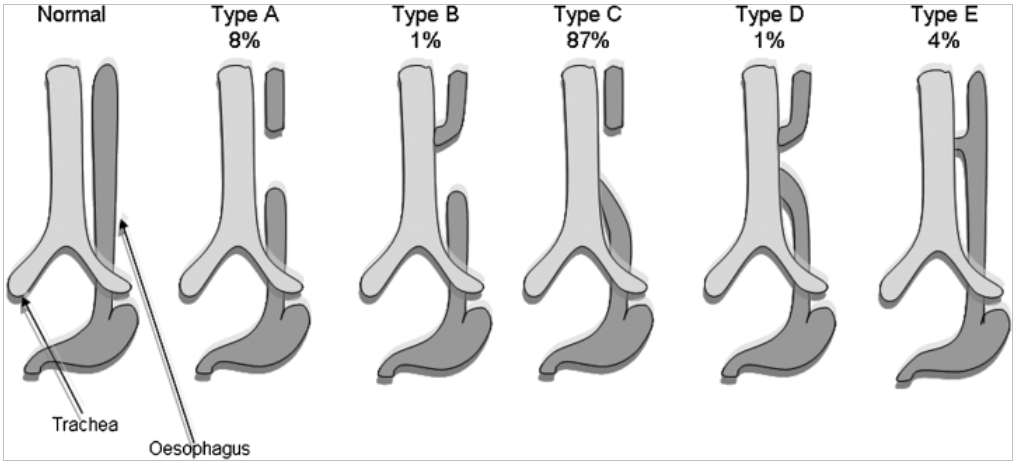

Figure 1.1: Relative occurrence of the various types of esophageal atresia (EA) with and without tracheoesophageal fistula (TEF) (adapted from Geneviève et al. (2007))

The common method to repair esophageal atresia is to connect the esophageal segments by primary anastomosis, but this method is very difficult to perform with large gap atresias. A viable alternative is the implantation of tissue engineered esophagi (Saxena et al., 2010).
At this stage of development of this method, ovine esophageal epithelial cells (OEEC) were seeded onto collagen scaffold sheets. These sheets were wrapped around sterile endotracheal tubes to get a tubular construction, and implanted into the omentum of the lambs.

After 8 to 10 weeks they were removed for histologic and morphologic evaluations (Saxena et al., 2010).
To ensure that these esophagi show the same biomechanical behavior as their naturally grown counterparts, the biomechanical behavior of ovine esophagi has to be investigated.

1.4 Anatomy of the esophagus

1.4.1 The gastrointestinal system of the sheep

The gastrointestinal tract is a continuous channel through the body from the mouth to the anus. The gastrointestinal anatomy shows large inter-species variations in structure and function due to the different kind of diets of the species (Gregersen, 2003).
In general, the alimentary tube can be divided into four parts:

- oral cavity and pharynx
- esophagus and stomach
- small intestine
- large intestine

The oral cavity, the first part of the alimentary tube, is surrounded by the lips, the chops, the palatine and the tongue together with the bottom of the mouth. Here the food is masticated by the teeth. Ruminant animals masticate only superficial, which allows foreign particles to get into the stomach. The tongue transports the food to the pharynx, where it can be swallowed and transported with peristaltic movements through the esophagus into the stomach (Loeffler, 1991).
The stomach of ruminant animals consists of four parts: the rumen, the reticulum, the omasum and the abomasum. The first three stomachs don't have glands, in contradiction to the abomasum, which correspond to the stomach of other animals. The function of rumen, reticulum and omasum is the rearrangement and fermentation of the food. In newborns, they are very small, and the milk get through a channel directly into the abomasum, where it coagulates with the help of the lab-ferment (Loeffler, 1991).
The small intestine of the sheep has a mean length of 25 m. The liquid content of the stomach is transported through the small intestine with peristatltic movements, while enzymes from the pankreas and the intestine and gall from the liver are added to digest the food. To improve the resorption of nutrients and water, the mucosa of the small intestine has villi. These villi increase the surface of the mucosa up to 600 times (Loeffler, 1991).
The large intestine of the sheep has a length on approximatly 5 m. Here the digestion ends, while more water is resorbated and the feces are formed and laxated by the rectum (Loeffler, 1991).
Figure 1.2 gives a schematic view of the gastrointestinal tract of the sheep.

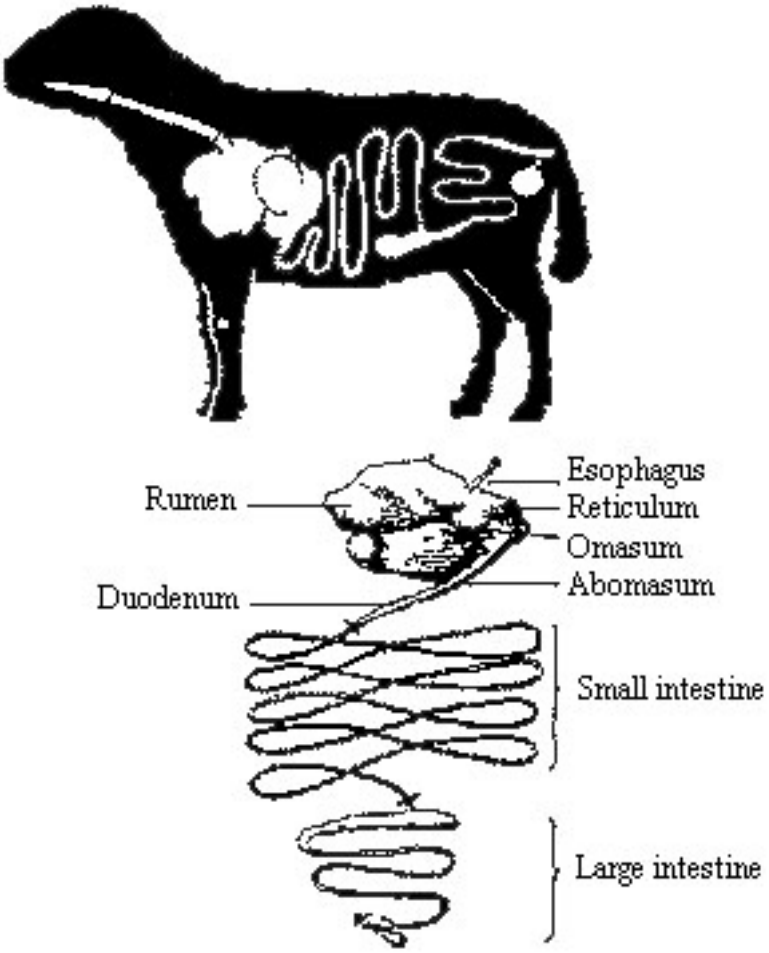

Figure 1.2: Gastrointestinal tract of the sheep (adapted from Mann (1962))

1.4.2 The esophagus

The esophagus transports the food through muscle contractions from the pharynx to the stomach. It consists of multiple layers, which is typically for the whole gastrointestinal system (Fig. 1.3). The most inner layer is the so-called mucosa, followed by the submucosa. The mucosa is a layer of epithelium cells, which form a continuous and homogeneous sheet. The submucosa is a broad zone of connective tissue, consisting of collagen and elastic fibres including a large amount of water. It allows the mucosa to move freely. Attached to the submucosa is the muscle layer, which is the source of the peristaltic movements. While humans have both striated and smooth muscle cells, ruminant animals like sheeps have only striated muscles, and can conduct antiperistaltic movements to transport the food back into the mouth to ruminate it. The muscle layer is surrounded by a layer of connective tissue, the so-called adventitia, which supports the flexibility of the esophagus and its integration in the thorax (Loeffler, 1991; Gregersen, 2003; Faller, 2004).

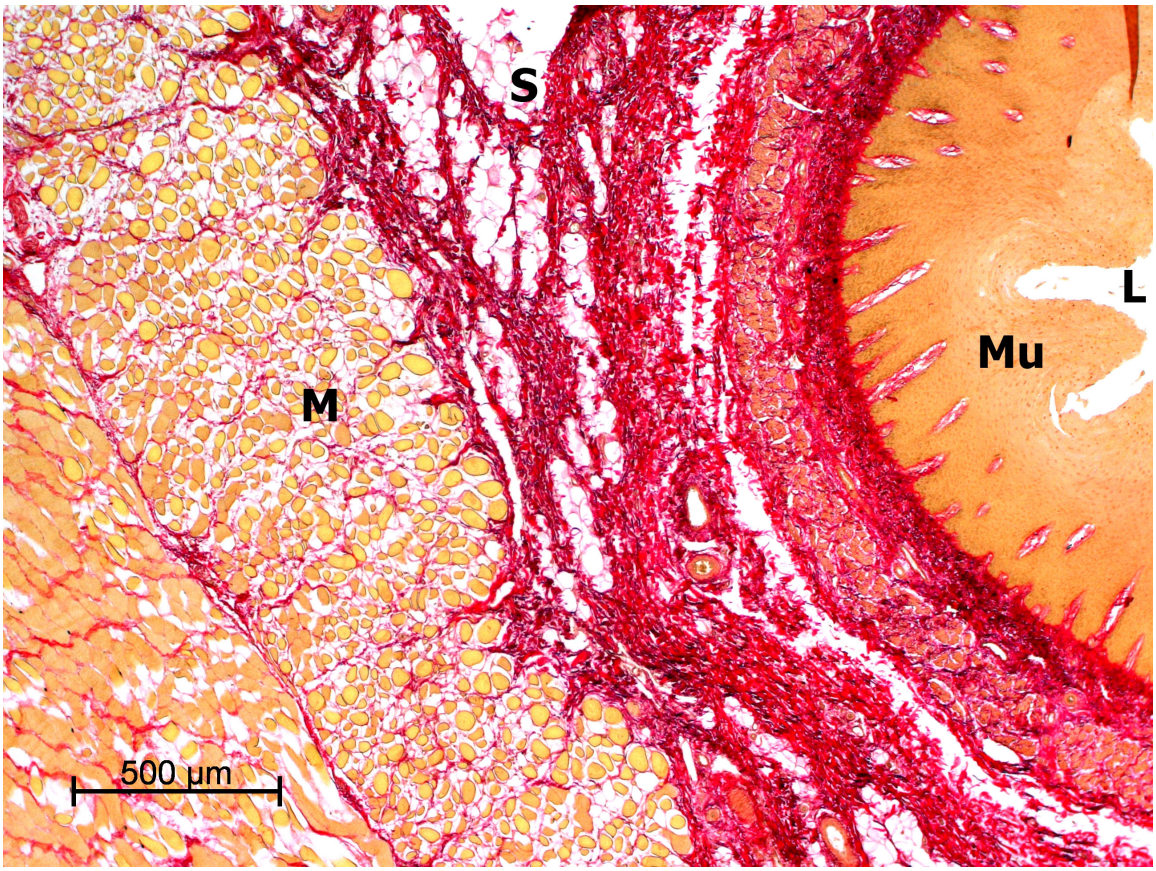

Figure 1.3: Histological view of the ovine esophagus displaying the muscle layer (M), the submucosa (S), the mucosa (Mu), and the lumen (L) with permission from G. Zeindlinger

1.5 General characteristics of esophageal soft tissue

1.5.1 Material symmetries

Due to the complex assembly of the esophageal layers, the mechanical behavior of the esophagus is anisotropic (Gregersen, 2003). Anisotropy means, that the mechanical behavior depends on the direction. While the collagen fibrils in the mucosal layer are organized in a loose and random network, the collagen fibrils in the submucosa are organized in thick fibres arranged in a criss-cross pattern. The muscle layer consists of two layers, which are orientated in the circumferential and axial directions, respectively (Natali et al., 2009). Yang et al. (2006a) observed a large disparity in the extensibility between the circumferential and axial directions of porcine esophagi.

1.5.2 Heterogeneity

The esophagus consists of multiple layers, mucosa, submucosa and muscle. The heterogeneity of the wall is only in radial direction present. Along the axial and circumferential direction the esophagus can be treated as a homogenous organ. This heterogeneous assembling suggests that the stress distribution across the whole wall is also heterogeneous therefore the material constants likely differ between the layers (Yang et al., 2006d).

1.5.3 Nonlinearity

Biological soft tissues like the esophagus show a nonlinear stress-stretch behavior. This means, that the tissue is compliant for small stresses and becomes stiffer with higher levels of stress. The reason for this behavior lies in the microscopic structure of the tissue. The extracellular matrix of biological tissues contains collagen fibrils. Most fibrillar collagen is typically undulated in the unloaded configuration. If a force is acting on the fibers, they straighten until they are aligned along the direction of the force. In this configuration, the collagen is much stiffer than in the wavy configuration (Holzapfel et al., 2000; Humphrey, 2002).

1.5.4 Viscoelasticity

A material can be divided into the following properties: **elastic** properties (spring), **viscous** properties (dashpot) and **plastic** properties (glider). Nearly all materials are mixtures of these properties, and behave viscoelastically, elastoplastically or viscoplastically (Zachow, 1997).
Most, if not all biological tissues show viscoelastical behavior, a combination of viscous and elastic behavior. This means, that the occuring stress depends on the applied strain, as well as on the rate of the strain. If a material is strained, the response is time-dependent. A suddenly applied and maintained constant stress will induce a stress decreasing response with time which is called **stress relaxation**. A suddenly applied and maintained stress

level will induce a continuous deforming of the material which is called **creep**. During cyclic loading, the stress-strain relationship is different in the loading process than in the unloading process. This phenomenon is called **hysteresis** (Fung, 1993).

1.5.5 Preconditioning

Preconditioning is very important in mechanical testing of living tissues *in vitro*. For this the mounted samples have to be repeatedly loaded and unloaded until the stress-strain relationship becomes reproducible. The necessary number of cycles depends on the tissue and the preparation method. The reason, why preconditioning has to be performed, is because the internal structure changes during the cycling. By repeated cycling, a steady state can be reached at which no further change will occur until changing the cyclic routine. In esophageal tissues, at least 3-10 cycles are needed, to get reproducible stress/strain curves (Fung, 1993; Gregersen, 2003).

1.5.6 Incompressibility

Esophagi consist like all other biological tissue of solid parts (collagen, muscle cells) and liquid parts (intra- and extra cellular water). In the linear elastic case, incompressibility means, that the poisson number (ratio of relative change of thickness to relative change of length) has to be 1/2 and the compression modulus has to be infinitely big. Thats why no real material can be ideally incompressible. If a material can be called incompressible depends on the ratio of the compression modulus to the shear modulus (Holzapfel et al., 2000; Sommer, 2003).

1.5.7 Residual strains

If someone wants to measure the stress-strain relationships of a tissue, these relationships have to be measured relative to the so-called **zero-stress state**, a state where no internal or external forces deform the tissue. In 1983 it was reported by Vaishnav and Vossoughi (1983) , and Fung (1983) independently, that biological organs are not free of stress when all external forces were removed, which means, that the zero-stress state is not the same as the **no-load state**, and that so-called **residual strains** occur in tissue even without external forces. Due to the three-dimensional nature of biological organs, residual stresses and strains exist in all three, i.e. circumferential, axial and radial directions. Residual stress occurs to reduce stress gradients across the wall thickness (Fung, 1993; Gregersen, 2003).

1.6 Basics of biomechanics

To describe the motion of a body, several models can be used:

- The mass point model for translations with 3 degrees of freedom,
- The rigid body model for additional rotations with 6 degrees of freedom,
- The atomistic model for deformations of bodies at a microscopic scale, used in solid-state physics,
- The continuum model for deformations of bodies at a macroscopic scale, used in biomechanics.

In the continuum model, the space is completely filled by the body. Macroscopic mechanical quantities, e.g. mass density, velocity, etc., are continuous functions of location and time, and equations of motion are partial differential equations. A point in space in the continuum model is considered to be an element of volume around that point. This element of volume has to be on the one hand big enough, to define macroscopical quantities, like the mass density or the hydrostatical pressure, on the other hand it has to be small enough, that the analytical treatment as infinitesimal variable is justified. This can be assured by defining $\delta/\Delta \ll 1$, with δ the characteristic length scale of a microstructure of the material and Δ the length scale of the macroscopic structure to be investigated.
To describe a problem with the mass point or the rigid body model, a kinematical concept, knowledge of the ocurring forces, balance relations or laws of conservation, as well as initial and boundary conditions are needed. For describing a mechanical problem with continuum mechanics, the displacement of points in space, described by a vector, has to be replaced by a deformation tensor, and a stress tensor has to be established for describing forces inside or at the boundaries of a deformable body. The deformability has to be considered in the balance relations, and material equations, respectively constitutive relations have to be formulated, to connect deformation and stress (Holzapfel, 2000; Humphrey, 2002; Sommer, 2003).

1.6.1 Kinematics

Kinematics is defined as the study of motion. The term 'motion' includes the current movement of the body (e.g., the velocity or acceleration of material particles in a body), as well as the relative change of the position of a particle from a reference configuration into a current configuration. The reference configuration Ω_0 (at time $t = 0$) is defined via the position vector $\mathbf{X}$ and the current configuration Ω_t (at time t) via the position vector $\mathbf{x}$ and the time t.
The position of a particle $\mathbf{x}$ at time t depends on the original position $\mathbf{X}$: $\mathbf{x} = \boldsymbol{\chi}(\mathbf{X}, t)$. Because the motion of a individual particle is of main interest, the differential line segments from one configuration to another has to be observed. Hence, the differential line

segment in the reference configuration is defined as d**X** and the differential line segment in the current configuration is defined as d**x**. These two line elements are related via the **deformation gradient F**. At each time,

$$\mathrm{d}\mathbf{x} = \mathbf{F}(\mathbf{X}, t)\mathrm{d}\mathbf{X}, \quad \mathrm{d}x_i = F_{iA}\mathrm{d}X_A, \tag{1.1}$$

with the symbolic notation on the left, and the index notation on the right side. The deformation gradient **F** is a second-order tensor. Because **x** is a function of **X**, at each fixed time *t*, the chain rule requires

$$\mathrm{d}\mathbf{x} = \frac{\partial \mathbf{x}}{\partial \mathbf{X}}\mathrm{d}\mathbf{X}, \quad \mathrm{d}x_i = \frac{\partial x_i}{\partial X_A}\mathrm{d}X_A. \tag{1.2}$$

Comparing equations (1.1) and (1.2), reveals that

$$\mathbf{F} = \frac{\partial \mathbf{x}}{\partial \mathbf{X}}, \quad F_{iA} = \frac{\partial x_i}{\partial X_A}. \tag{1.3}$$

The physical components of **F** can be written in matrix notation as following:

$$F_{iA} = [\mathbf{F}] = \begin{bmatrix} \frac{\partial x_1}{\partial X_1} & \frac{\partial x_1}{\partial X_2} & \frac{\partial x_1}{\partial X_3} \\ \frac{\partial x_2}{\partial X_1} & \frac{\partial x_2}{\partial X_2} & \frac{\partial x_2}{\partial X_3} \\ \frac{\partial x_3}{\partial X_1} & \frac{\partial x_3}{\partial X_2} & \frac{\partial x_3}{\partial X_3} \end{bmatrix} = \begin{bmatrix} \lambda_1 & 0 & 0 \\ 0 & \lambda_2 & 0 \\ 0 & 0 & \lambda_3 \end{bmatrix}, \tag{1.4}$$

with λ_1, λ_2 and λ_3 the stretches in the three directions of the main axis x, y and z.

The deformation gradient **F** can be decomposed via

$$\mathbf{F} = \mathbf{R}\mathbf{U} = \mathbf{v}\mathbf{R}, \tag{1.5}$$

where **R** represents the rigid body motion with $\mathbf{R}^T\mathbf{R} = \mathbf{I}$. **U** is defined in the reference configuration Ω_0 as the **right (or material) stretch tensor**, and **v** is defined in the current configuration Ω_t as the **left (or spatial) stretch tensor**. Since **U** is a real symmetrical and positive definite second-order tensor, it has three real positive eigen-values λ_i and three associated orthonormal eigenvectors $\mathbf{N}_i$. The spectral decomposition of the right stretch tensor is:

$$\mathbf{U} = \sum_{i=1}^{3} \lambda_i \mathbf{N}_i \otimes \mathbf{N}_i, \tag{1.6}$$

with $\lambda_i = \partial x_i / \partial X_i$ the **stretch ratios**.
A stretch ratio is not a physical value, but a mathemathical concept to describe deformable bodies in kinematics. A valuable stretch ratio has to fulfill the following characteristics:

(i) It has to establish a relationship between the differential line segment d**X** of the reference configuration and d**x** of the current configuration, which covers occurring changes of length and angle in the continuum.

(ii) It has to be independent against coordinate transformations and

(iii) Invariant against rigid body rotations.

The deformation gradient **F** is not the best measure for analysis in elasticity, because it contains a rigid body rotation, as can be seen in eq. (1.5). This rigid body rotation can be eliminated as following:

$$\mathbf{F}^T\mathbf{F} = (\mathbf{RU})^T\mathbf{RU} = \mathbf{U}^T\mathbf{R}^T\mathbf{RU} = \mathbf{U}^T\mathbf{IU} = \mathbf{U}^T\mathbf{U} = \mathbf{U}^2 = \mathbf{C} \tag{1.7}$$

with **C** the **right Cauchy-Green tensor**, $\mathbf{F}^T$ the **transposed deformation gradient** and **I** the **unit tensor**. **C** is a symmetrical second-order tensor, independent of rigid body rotations, and a spectral decomposition from eq. (1.7) and eq. (1.6):

$$\mathbf{C} = \sum_{i=1}^{3} \lambda_i^2 \mathbf{N}_i \otimes \mathbf{N}_i, \tag{1.8}$$

It is often convenient, to define the so-called **Green-Lagrangian strain tensor E**, that equals 0 when there is no deformation:

$$\mathbf{E} = \frac{1}{2}(\mathbf{C} - \mathbf{I}) \quad \text{or} \quad \mathbf{E} = \frac{1}{2}(\mathbf{F}^T\mathbf{F} - \mathbf{I}). \tag{1.9}$$

The right Cauchy-Green tensor **C** can be diagonalized to:

$$[\mathbf{C}] = \begin{bmatrix} \lambda_1^2 & 0 & 0 \\ 0 & \lambda_2^2 & 0 \\ 0 & 0 & \lambda_3^2 \end{bmatrix}, \tag{1.10}$$

and the Green-Lagrangian tensor **E** to:

$$[\mathbf{E}] = \frac{1}{2}\begin{bmatrix} \lambda_1^2 - 1 & 0 & 0 \\ 0 & \lambda_2^2 - 1 & 0 \\ 0 & 0 & \lambda_3^2 - 1 \end{bmatrix}. \tag{1.11}$$

The diagonal elements of **E** are:

$$E_{ii} = \frac{1}{2}(\lambda_i^2 - 1) \quad i \in 1, 2, 3. \tag{1.12}$$

With the implementation of the **displacement vector** $\mathbf{u} = \mathbf{x} - \mathbf{X}$ respectively $\mathrm{d}\mathbf{u} = \mathrm{d}\mathbf{x} - \mathrm{d}\mathbf{X}$, **F** can be written as:

$$\mathbf{F} = \mathbf{I} + \mathbf{H}, \tag{1.13}$$

with $\mathbf{H} = \partial\mathbf{u}/\partial\mathbf{X}$ the **displacement gradient**. The combination of equations (1.9) and (1.13) changes the Green-Lagrangian tensor **E** to:

$$\mathbf{E} = \frac{1}{2}(\mathbf{H} + \mathbf{H}^T + \mathbf{H}^T\mathbf{H}). \tag{1.14}$$

If the deformation and the rigid body rotations are both small ($\mathbf{F} \simeq \mathbf{I}$ and $\mathbf{R} \simeq \mathbf{I}$), then $\partial\mathbf{u}/\partial\mathbf{X} \simeq \partial\mathbf{u}/\partial\mathbf{x}$ and the quadratic terms in eq. (1.14) become negligible in comparison to the linear terms. This leads to the definition of the so-called **infinitesimal (or linearized) strain tensor** ε:

$$\boldsymbol{\varepsilon} = \frac{1}{2}(\mathbf{H} + \mathbf{H}^T), \tag{1.15}$$

whereby it is seen that $\boldsymbol{\varepsilon}$ is only an approximative measure of particular measures of strain, unlike $\mathbf{E}$ which is exact within the context of the continuum theory. $\boldsymbol{\varepsilon}$ can also be written as:

$$\boldsymbol{\varepsilon} = \frac{1}{2}(\mathbf{F} + \mathbf{F}^T) - \mathbf{I}, \tag{1.16}$$

$$[\boldsymbol{\varepsilon}] = \begin{bmatrix} \lambda_1 - 1 & 0 & 0 \\ 0 & \lambda_2 - 1 & 0 \\ 0 & 0 & \lambda_3 - 1 \end{bmatrix}, \tag{1.17}$$

with the diagonal elements $\varepsilon_{ii} = \lambda_i - 1$.

The advantage of the linearized strain tensor $\boldsymbol{\varepsilon}$ is, that strains and shear strains are uncoupled, despite to $\mathbf{E}$. The main diagonal elements state the strains along the coordinate axis, and the non-diagonal elements state the shear strains between the axis. The disadvantage of $\boldsymbol{\varepsilon}$ is, that it is not independent of rigid body rotations, since it depends linearly on $\mathbf{F}$, and that it is only approximately right for small deformations, because:

$$E_{ii} = \frac{1}{2}(\lambda_i^2 - 1) = \frac{1}{2}\left[\left(\frac{\partial x_i}{\partial X_i}\right)^2 - 1\right] = \frac{1}{2}\left[\left(\frac{\partial (X_i + u_i)}{\partial X_i}\right)^2 - 1\right] = \frac{\partial u_i}{\partial X_i} + \frac{1}{2}\left(\frac{\partial u_i}{\partial X_i}\right)^2 = (\lambda_i^2 - 1) + \frac{1}{2}\left(\frac{\partial u_i}{\partial X_i}\right)^2 = \varepsilon_{ii} + O(u_i^2) \tag{1.18}$$

For small displacements u_i, the quadratic term can be neclected, and ε_{ii} equals approximately E_{ii}. This assumption however, can only be made with small stretches of technical materials, but not with highly deformable biological tissues.

With the deformation gradient $\mathbf{F}$, the kinematical relation between the differential line segments, as well as the relation between the differential area and volume segments, can be obtained (Table 1.1) (Holzapfel, 2000; Humphrey, 2002; Sommer, 2003).

Table 1.1: Kinematical relations between reference and current configuration with **a** the area segment vector in the current configuration, **A** the area segment vector in the reference configuration, v the volume segment in the current configuration, and *V* the volume segment in the reference configuration.

differential line segment	$\mathrm{d}\mathbf{x} = \mathbf{F}\mathrm{d}\mathbf{X}$
differential area segment	$\mathrm{d}\mathbf{a} = (det\mathbf{F})\mathbf{F}^{-T}\mathrm{d}\mathbf{A}$
differential volume segment	$\mathrm{d}v = (det\mathbf{F})\mathrm{d}\,V$

1.6.2 Forces and stresses

A force is considered to be an action of one body on another, that is a vectorial 'push' or 'pull'. Forces can be divided into to two general types:
(i) **body forces**, like gravity or electromagnetical forces, acting on all material particles in a body without physical contact, and
(ii) **surface forces**, like pressure or frictional forces, acting through physical contact on a body through its bounding surfaces.
Since many forces act on a body through a surface area, it is useful to define a **traction vector t** as:

$$\mathbf{t} = \lim_{\Delta a \to 0} \left(\frac{\Delta \mathbf{f}}{\Delta a} \right) = \frac{\mathrm{d}\mathbf{f}}{\mathrm{d}a}, \tag{1.19}$$

with d**f** a differential force vector and d*a* a differential area, both defined in the current configuration Ω_t. The orientation of d*a* is given by the outward unit normal vector **n**.
The **Cauchy stress tensor** $\boldsymbol{\sigma}$ is defined as the connection of the traction vector or **Cauchy traction vector t** with the outward unit normal vector **n** of the differential area d*a*,

$$\mathbf{t} = \boldsymbol{\sigma}\mathbf{n} \quad , \quad t_j = \sigma_{ji} n_i. \tag{1.20}$$

Here, the *i* subscript in the Cauchy stress denotes the orientation of the area on which the force acts, and the *j* subscript denotes the orientation of the applied force.

The Cauchy stress $\boldsymbol{\sigma}$ is defined as the force in the current configuration, acting on a body over a current area. Therefore it is defined in the current configuration Ω_t, and is called the true stress, which is actually 'felt' by the material. With the conservation of angular momentum, the symmetry of $\boldsymbol{\sigma}$ can be shown. As a symmetrical second-order tensor it has three real eigen-values and six independent components, with the Cartesian representation:

$$\boldsymbol{\sigma} = \sigma_{ij} \mathbf{e}_i \otimes \mathbf{e}_j. \tag{1.21}$$

In solid mechanics, it is not always possible to know what configuration a body will assume after the application of loads, thus, it can be difficult to define or measure $\boldsymbol{\sigma}$. Therefore,

it is useful to define another measure of stress with respect to the reference configuration Ω_0. For this, the actual force vector d**f** has to be translated from its point of application **x** in the current configuration Ω_t to the corresponding point **X** in the reference configuration Ω_0. Now, a new **traction vector T** and a new stress tensor **P**, that transforms **N** into **T**, can be defined:

$$\mathbf{T} = \frac{\mathrm{d}\mathbf{f}}{\mathrm{d}A} \quad , \quad \mathbf{T} = \mathbf{P}\mathbf{N}, \tag{1.22}$$

with d*A* the differential area segment, defined by the outward unit normal vector **N**, and **P** the so-called **first Piola-Kirchhoff stress tensor**, defined as the actual force, acting on the unit area in the reference configuration Ω_0. **P** is only a mathemathical construct without any physical reality, consisting of parts of the current and the reference configuration, which makes it very convinient for experimental measurements. It is not symmetric (i.e., $\mathbf{P} \neq \mathbf{P}^T$) and has nine independent components.
There is also the motivation to look for a symmetric second-order tensor, defined completely in the reference configuration. For this, a 'fictitious' force has to be defined in the reference configuration, transformed with $\mathbf{F}^{-1}$, the inverse of the deformation gradient **F**, from the current to the reference configuration: $\mathrm{d}\tilde{\mathbf{f}} = \mathbf{F}^{-1}\mathrm{d}\mathbf{f} = \mathrm{d}\mathbf{f}\mathbf{F}^{-T}$. Now, a new **traction vector** $\tilde{T}$ and a new stress tensor **S**, connecting **N** and $\tilde{\mathbf{T}}$, can be defined:

$$\tilde{\mathbf{T}} = \frac{\mathrm{d}\tilde{\mathbf{f}}}{\mathrm{d}A} \quad , \quad \tilde{\mathbf{T}} = \mathbf{S}\mathbf{N}. \tag{1.23}$$

S is called the **second Piola-Kirchhoff stress tensor**, a symmetrical second-order tensor, existing in the reference configuration.

The question is, wether these three measures of stress are independent. Since

$$\mathrm{d}\mathbf{f} = \mathbf{t}\mathrm{d}a = \boldsymbol{\sigma}\mathbf{n}\mathrm{d}a, \tag{1.24}$$

and

$$\mathrm{d}\mathbf{f} = \mathbf{T}\mathrm{d}A = \mathbf{P}\mathbf{N}\mathrm{d}A, \tag{1.25}$$

follows with **Nanson's relation** ((Humphrey, 2002), p. 77)

$$\mathbf{n}\mathrm{d}a = J\mathbf{F}^{-T}\mathbf{N}\mathrm{d}A \rightarrow \mathbf{N}\mathrm{d}A = \frac{1}{J}\mathbf{F}^{-T}\mathbf{n}\mathrm{d}a, \tag{1.26}$$

$$\boldsymbol{\sigma}\mathbf{n}\mathrm{d}a = \frac{1}{J}\mathbf{P}\mathbf{F}^{T}\mathbf{N}\mathrm{d}A \rightarrow \boldsymbol{\sigma} = \frac{1}{J}\mathbf{P}\mathbf{F}^{T}, \tag{1.27}$$

with *J* = det **F** the Jacobian of **F**. This shows, that all stress tensors are interrelated and contain all the same information. Table 1.2 gives an overview of these relations (Holzapfel, 2000; Humphrey, 2002; Sommer, 2003).

Table 1.2: Relations between the Cauchy stress tensor $\boldsymbol{\sigma}$, the first Piola-Kirchhoff stress tensor $\mathbf{P}$ and the second Piola-Kirchhoff stress tensor $\mathbf{S}$

	Configuration	f($\boldsymbol{\sigma}$)	g($\mathbf{P}$)	h($\mathbf{S}$)
$\boldsymbol{\sigma}$	Ω_t	$\boldsymbol{\sigma}$	$J^{-1}\mathbf{P}\mathbf{F}^T$	$J^{-1}\mathbf{F}\mathbf{S}\mathbf{F}^T$
$\mathbf{P}$	Ω_0, Ω_t	$J\boldsymbol{\sigma}\mathbf{F}^{-T}$	$\mathbf{P}$	$\mathbf{F}\mathbf{S}$
$\mathbf{S}$	Ω_0	$J\mathbf{F}^{-1}\boldsymbol{\sigma}\mathbf{F}^{-T}$	$\mathbf{F}^{-1}\mathbf{P}$	$\mathbf{S}$

1.6.3 Balance equations

The main task of continuum mechanics is to calculate the motion of continous bodies with given initial and boundary conditions. The combination of the general balance equations and the material specific constitutive equations yields the needed field equations.

There are five fundamental postulates or laws of conservation in continuum mechanics:

- **Conservation of mass**
- **Conservation of linear momentum**
- **Conservation of angular momentum**
- **Conservation of energy**
- **The entropy inequality**

Only conservation of mass and linear momentum will be discussed here, since the other ones have no important influence on the measurements of this work.

Conservation of mass

In non-relativistic physics, conservation of mass requires, that the total mass of a body is the same in the reference configuration Ω_0 and in the current configuration Ω_t:

$$m = \int_{\Omega_0} \rho_0 \mathrm{d}V = \int_{\Omega_t} \rho \mathrm{d}V = const. > 0, \tag{1.28}$$

with ρ_0 the mass density in Ω_0 and ρ the mass density in Ω_t. The volumes of the reference and the current configuration are related via $dv = JdV$, changing the equation above to:

$$\int_{\Omega_0} (\rho_0 - \rho J)\mathrm{d}V = 0 \quad \forall \Omega_0. \tag{1.29}$$

Because of the time independence of ρ_0,

$$\frac{\mathrm{d}\rho_0}{\mathrm{d}t} = \frac{\mathrm{d}}{\mathrm{d}t}(\rho J) = 0, \tag{1.30}$$

and with the relation

$$\frac{\mathrm{d}J}{\mathrm{d}t} = J\mathrm{div}\mathbf{v}, \tag{1.31}$$

with **v** the velocity:

$$\frac{\mathrm{d}}{\mathrm{d}t}(\rho J) = \frac{\mathrm{d}\rho}{\mathrm{d}t}J + \rho\frac{\mathrm{d}J}{\mathrm{d}t} = J\left(\frac{\mathrm{d}\rho}{\mathrm{d}t} + \rho\mathrm{div}\mathbf{v}\right) = 0, \tag{1.32}$$

respectively

$$\frac{\mathrm{d}\rho}{\mathrm{d}t} + \rho\mathrm{div}\mathbf{v} = 0, \tag{1.33}$$

because $J = det\mathbf{F} > 0$.

With $\mathrm{d}\rho/\mathrm{d}t = \partial\rho/\partial t + \mathbf{v}\mathrm{grad}\rho$, the known **continuity equation**

$$\frac{\partial\rho}{\partial t} + \mathrm{div}(\rho\mathbf{v}) = 0, \tag{1.34}$$

the differential form of the conservation of mass, can be obtained. If the continuum is incompressible, a simple form of the continuity equation is valid, because of the constant density $d\rho/dt = 0$:

$$\mathrm{div}\mathbf{v} = 0. \tag{1.35}$$

Conservation of linear momentum

The linear momentum, mass m times velocity **v**, is a vector with the density $\mathbf{g} = \rho\mathbf{v}$. The second Newtonian axiom 'change of momentum in time equals sum of all acting forces' can be written as:

$$\frac{\mathrm{d}}{\mathrm{d}t}\int_{\Omega_t}\rho\mathbf{v}\mathrm{d}v = \int_{\Omega_t}\rho g\mathrm{d}v + \int_{\partial\Omega_t}\mathbf{t}\mathrm{d}a, \tag{1.36}$$

with **v** the velocity, g the gravitational acceleration, $\mathbf{t} = \boldsymbol{\sigma}\mathbf{n}$ with **t** the Cauchy stress vector, $\boldsymbol{\sigma}$ the Cauchy stress tensor and **n** the unit normal vector. Application of the divergence theorem on the right integral and the observation of arbitrary parts of the body leads to the local form

$$\rho\frac{\mathrm{d}\mathbf{v}}{\mathrm{d}t} = \rho g + \mathrm{div}\boldsymbol{\sigma}, \tag{1.37}$$

of the **conservation of linear momentum**. This local form is also called spatial form of the **1. Cauchy equation of motion**. In the stationary case d*v*/d*t* = 0 and under disregard of the gravity, the **fundamental Cauchy equation of elastostatics**,

$$\mathrm{div}\boldsymbol{\sigma} = 0, \tag{1.38}$$

is given (Holzapfel, 2000; Humphrey, 2002; Sommer, 2003).

1.6.4 Incremental and finite material characteristics

Hookes' law connects the Cauchy stress tensor $\boldsymbol{\sigma}$ and the linearized strain tensor $\boldsymbol{\varepsilon}$ in the linear case like this:

$$\boldsymbol{\sigma} = \mathbb{C} : \boldsymbol{\varepsilon} \quad , \quad \sigma_{ij} = C_{ijkl} : \varepsilon_{kl}, \tag{1.39}$$

with $\mathbb{C}$ the **fourth order elasticity tensor**, with $3^4 = 81$ constant components in $\mathbb{R}^3$. Due to symmetries, the components can be reduced to 21 independent components in the most general anisotropic case, to nine with orthotropic material symmetries and to two with isometry. The problem is, that biological soft tissues show nonlinear behavior, and a linear-orthotropic model with only nine components would only be valid for incremental small parts.
Due to their almost elastic deformation behavior, it is better to describe biological tissues with so-called **elastic potentials**. The nonlinear and anisotropic mechanical behavior can be described with few **material parameters** and the shape of the used potential. A model based on a potential is called **hyperelastic**. The underlying idea of the elastic potential or **strain-energy function** is, that the deformation work is stored reversible in the body. Therefore a reference configuration is needed, where the stored energy is zero.
With elastic potentials, **constitutive equations** can be formulated, describing the relation between stress and strain tensors:

$$\mathbf{P} = \mathbf{P}(\mathbf{F}) = \frac{\partial \Psi}{\partial \mathbf{F}}, \tag{1.40}$$

respectively

$$\mathbf{S} = \mathbf{S}(\mathbf{E}) = \frac{\partial \Psi}{\partial \mathbf{E}}, \tag{1.41}$$

with $\mathbf{P}$ the first Piola-Kirchhoff stress tensor, $\mathbf{F}$ the deformation gradient, $\mathbf{S}$ the second Piola-Kirchhoff stress tensor, $\mathbf{E}$ the Green Lagrangian strain tensor and Ψ the strain-energy function. Strain and stress tensor are called **conjugated quantities**, because they are linked together via the strain-energy function Ψ.
In the literature, there are different potentials for modeling biological tissues. They are mostly phenomenological potentials, based on experimental data, and can be divided due to their mathemathical structur into polynomial, exponential, logarithmical and mixed potentials (Holzapfel, 2000; Holzapfel et al., 2000; Humphrey, 2002; Sommer, 2003).

2 Methods

2.1 Biomechanical methods

There are many methods to obtain biomechanical data from biological tissues. To get a good overview, it is practicable to put them in different categories, which are:

- *in vivo* and *in vitro*
- quasi-static and dynamic
- uni-, bi- and triaxial
- reversible and irreversible

The term *in vivo* refers to experiments obtained in a living organism, while *in vitro* means an experiment in a partial or dead organism (Wikipedia, 2011). Biomechanical measurements obtained in the *in vivo* gastrointestinal tract are for example the measurement of the motility including electromyography, manometry, transit time measurements, ultrasonography, radiographic methods and methods for recording the distensibility. Uni-, bi- and triaxial measurements have to be done *in vitro*, while balloon distension techniques can be obtained both *in vivo* and *in vitro* (Gregersen, 2003).

The difference between dynamic and quasi-static loading is, that dynamic loading is time-dependent and inertial effects influence the measurement. A quasi-static loading is in principle also not time-independent like a static load, but it is slow enough, that inertial effects can be ignored (Yavari, 2010). So, if we want to measure the stress-strain relationship of a biological tissue without dynamic effects disturbing it, the loading of the stress on the sample has to be slow enough to be quasi-static.

To obtain stress-strain relationship data *in vitro*, there are three important methods. For uniaxial tests, small strips of tissues are mounted between two fixing clamps and by increasing the length of the strips, the occuring force is measured. While it is a very simple test, where the stress-strain relationship can easily be obtained, there are also some disadvantages. One is, that the structural integrity of the organ wall is not preserved and the sample is not necessarily in the zero-stress state. Another disadvantage is, that uniaxial tests are not physiological, since biological tissue is always loaded multiaxially *in vivo* (Gregersen, 2003).
To provide further information for the constitutive equation of a material, bi- and triaxial

tests are performed. In biaxial tests, forces are applied on flat sheets of biological tissue in two orthogonal directions and the strains are measured. Another form of biaxial tests are extension-inflation tests on tubular segments. Triaxial tests provide information in the axial, circumferential and shearing directions. For that a tubular segment of biological tissue is axially stretched, inflated and twisted (Gregersen, 2003).

While the uniaxial tensile tests, performed in this work, are reversible (no damage of the tissue), the rupture tests are, due to their nature, irreversible.

2.2 Materials

2.2.1 Equipment

The listed instruments and chemicals below are needed to perform the sample preparation and the tests and are thoroughly described later in the text.

Measuring instruments

- Testing device
  - μ-strain instrument Messphysik Series ME 30-34 (adapted for biomechanical tensile and inflation tests; capacity: $\pm$ 1 kN); Messphysik Laborgeräte G.m.b.H, A-8280 Fürstenfeld
- 2 External Digital Controller (axial displacement, pressure)
  - Doli EDC25; DOLI Elektronik G.m.b.H., D-81373 München
- Computer
- Videoextensometer
  - Videoextensometer ME - 46-350; Messphysik Laborgeräte G.m.b.H, A-8280 Fürstenfeld

  consisting of
  - CCD camera 1/3” (Mintron)
  - Objectives (25 mm, 50 mm)
  - Frame-Grabber
  - Video-Processor
  - User software: ‘Kunststoffzugversuch, Version 2.10.01’; ‘WinextNG, Version 5.26.0.0’
- Heatbath with heating coil

  - Lauda Ecoline-Einhängethermostat E 200; Lauda Dr. R. Wobser G.m.b.H. u. Co KG, D- 97912 Lauda-Königshofen

- Digital thermometer
- Calibration standard

Chemicals

- Phosphat buffered Saline PBS pH 7.2-7.4
  - 1.44 g $NaH_2PO_4 * 2H_2O$
  - 0.24 g KH_2PO_4
  - 0.2 g KCl
  - 8 g $NaCl$
  - 1000 ml H_2O
- EGTA

Used tools

- cutting board
- tweezers
- scissors
- scalpel
- punch cutter
- cup with screw cap
- Pencil and post-its
- pipette
- abrasive paper
- ribbon
- photo camera
- metal lineal
- super glue
- cord

2.2.2 Tissue requirements

For the correct measurements of the mechanical properties of the biological tissue, the samples have to satisfy various requirements.

Integrity of the tissue: No damage should occur to the sample during the slaughter or the sample preparation. Small damaged parts due to the slaughtering were removed and only faultless parts were used. Esophagi with big slaughter damages were disposed of. The preparation of the samples was obtained carefully to prevent damage. Also long time storage should be avoided, because of the onset of autolysis with time. Samples used in our tests were stored at maximum 3 days at $4\,^{\circ}\mathrm{C}$.

Geometry: To assure a homogenous stress-stretch behavior, the strip samples for the uniaxial tensile and rupture tests should have a so-called dog bone shape. This shape assures, that the mechanical strength of the sample is not disturbed by the fixing conditions (Principle of Saint-Venant), and that it ruptures at the point with the smallest cross-section (Sommer, 2003), (Brandenburger, 2011).

Structur: It is important for the tests, that the prepared samples represent the heterogenous and anisotropic structure of the esophagus. Therefore, an accurate dissection of the different layers and a comprehensible distinction between the axial and the circumferential direction of the esophagus are most important. A profound knowledge of the esophagus anatomy and a good practise in sample preparation assure, that these conditions are fulfilled.

Preconditioning: Preconditioning, as described in Chapter 1.5.5, is used to stabilize the mechanical response of the samples. In this work, the uniaxial tensile test samples were preconditioned four times, and the inflation tests samples were preconditioned nine times. The fifth, respectively tenth cycle of each test was used for measurement.

2.2.3 Esophagus

Fresh ovine esophagi were obtained from a local abattoir by Herwig Ainödhofer from the Medical University in Graz (Fig. 2.1). The samples were stored in PBS in the refrigerator at $4\,^{\circ}\mathrm{C}$. The tests were obtained between one and three days after the slaughter. For both the uniaxial tensile tests and the extension-inflation tests at least ten esophagi were needed to get statistically usable data. To measure the mechanics of the esophagi, the surrounding fat and connective tissue was removed with scissors (Fig. 2.2) and the samples were inspected for damage due to the slaughter. Parts with damaged or cut musclelayer could not be used and were removed. To clean the esophagi on the inside, water was pumped carefully through the tube with a pipette.

Figure 2.1: Fresh ovine esophagus before removing of surrounding fat and connective tissue

Figure 2.2: Ovine esophagus after removing of surrounding fat and connective tissue

2.2.4 Small intestine

Besides the esophagus, one sample of ovine small intestine was tested (Fig. 2.3). The intestine was obtained from the same abattoir as the esophagus and was stored in PBS in the freezer at $-18\,^{\circ}\mathrm{C}$ for seven days.

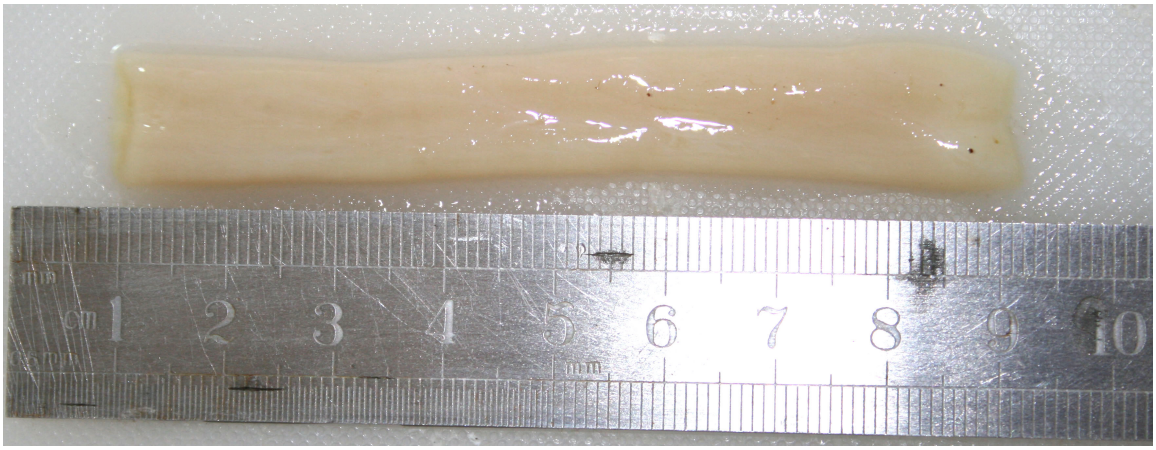

Figure 2.3: Cut part of the ovine small intestine

2.3 Experimental setup

2.3.1 Measuring equipment

Uniaxial tensile and rupture tests

The experimental setup for the uniaxial tensile and rupture tests consists of the strain instrument, an external digital controller and a computer for the data recording (Fig. 2.4). The strain instrument consists of two vertically moveable crossheads in a metal framework, which are moved diametrically opposed by a motor to assure the samples stay on the same height during the test. A load cell is positioned on the upper crossbar to measure the force acting on the sample. The sample is fixed by two fixing clamps which are connected to the upper and lower crossbar by two sample holder tubes. The stroke resolution of the fixing clamps is 0.4 μm (Sommer, 2003). During the tests a temperature controlled tissue bath sorrounds the sample to assure physiological conditions. This tissue bath consists of three liters PBS and 300 mg EGTA in a cuvette made of acrylic glass with internal dimensions of 150 $\times$ 150 $\times$ 160 mm and a wall thickness of 5 mm. An external digital controller, constructed for spindle-driven strain instruments, is monitoring the position of the crossbars and the gauge of the load cell and transmits these values to the computer. A CCD camera transmits a live view of the sample to the computer where the length and width of the sample are being measured. The computer than controlls the movement of the crossbars.

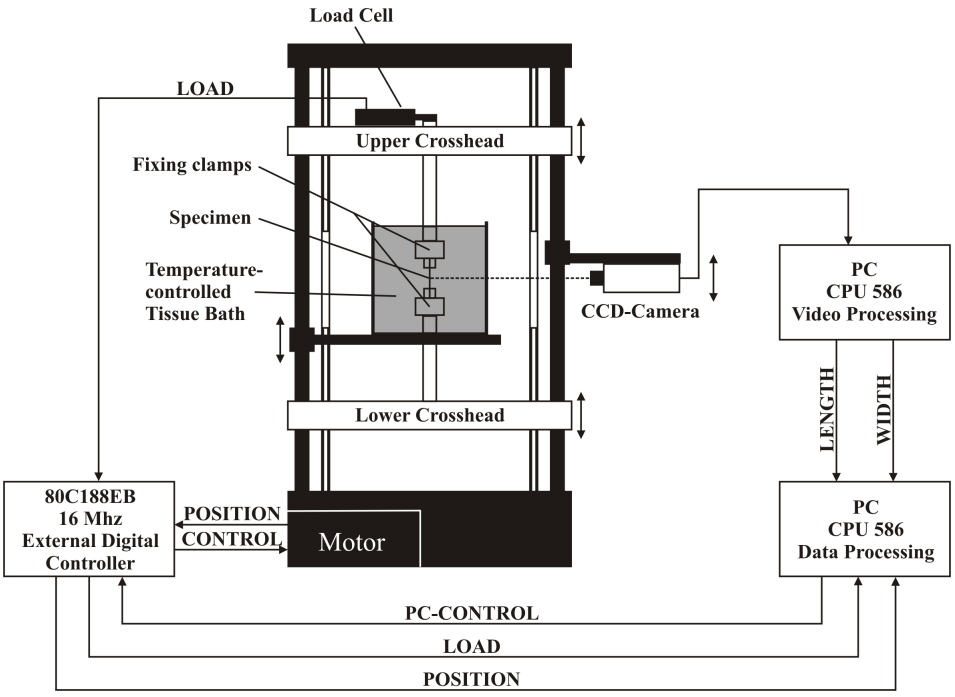

Figure 2.4: Schematic illustration of the uniaxial measuring equipment (adapted from Sommer et al. (2008))

Figure 2.5 shows the actual testing device, together with two lamps for adjusting the contrast and the heat bath in the background, which controlls the temperature of the tissue bath with a heating coil.

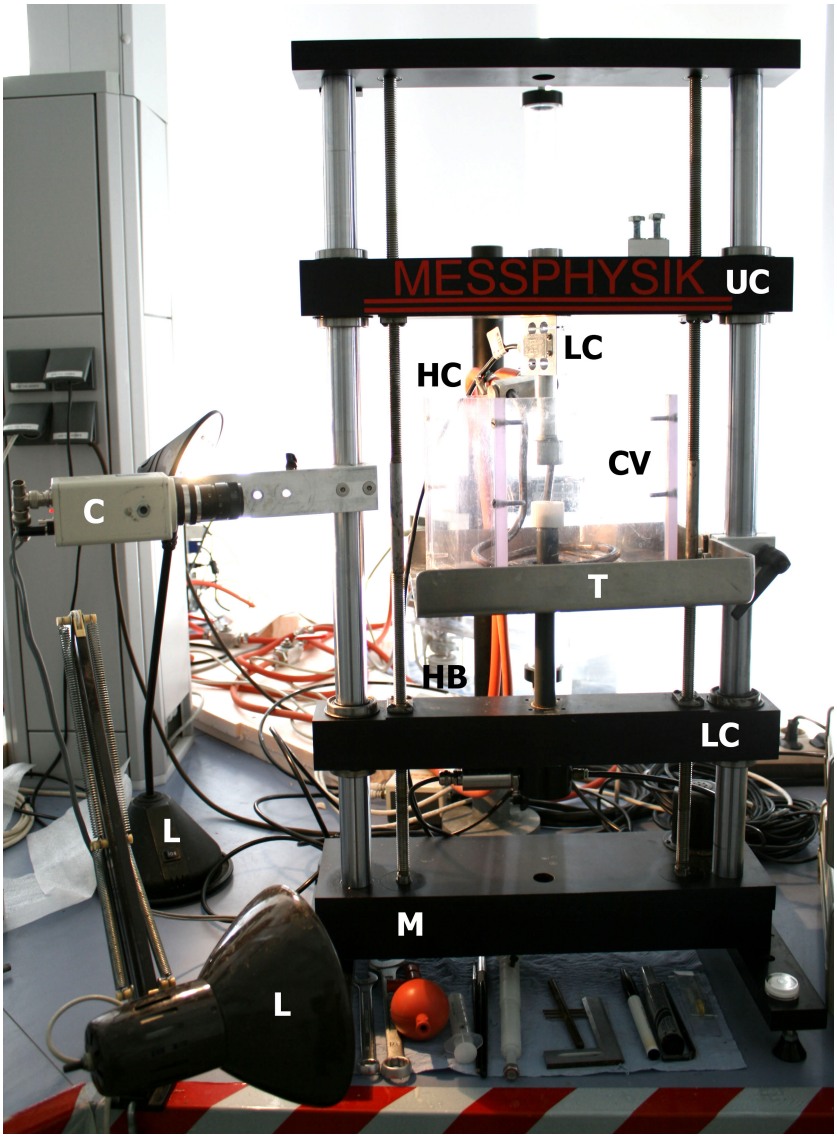

Figure 2.5: Experimental setup for tensile tests dispaying the load cell (LC), cuvette (CV), heating coil (HC), CCD camera (C), upper crosshead (UC), lower crosshead (LC), heatbath (HB), lamps (L), motor (M) and metal table (T)

Figure 2.6 is a detailed view of the strain instrument with the two fixing clamps attached to the lower sample holder tube and the load cell.

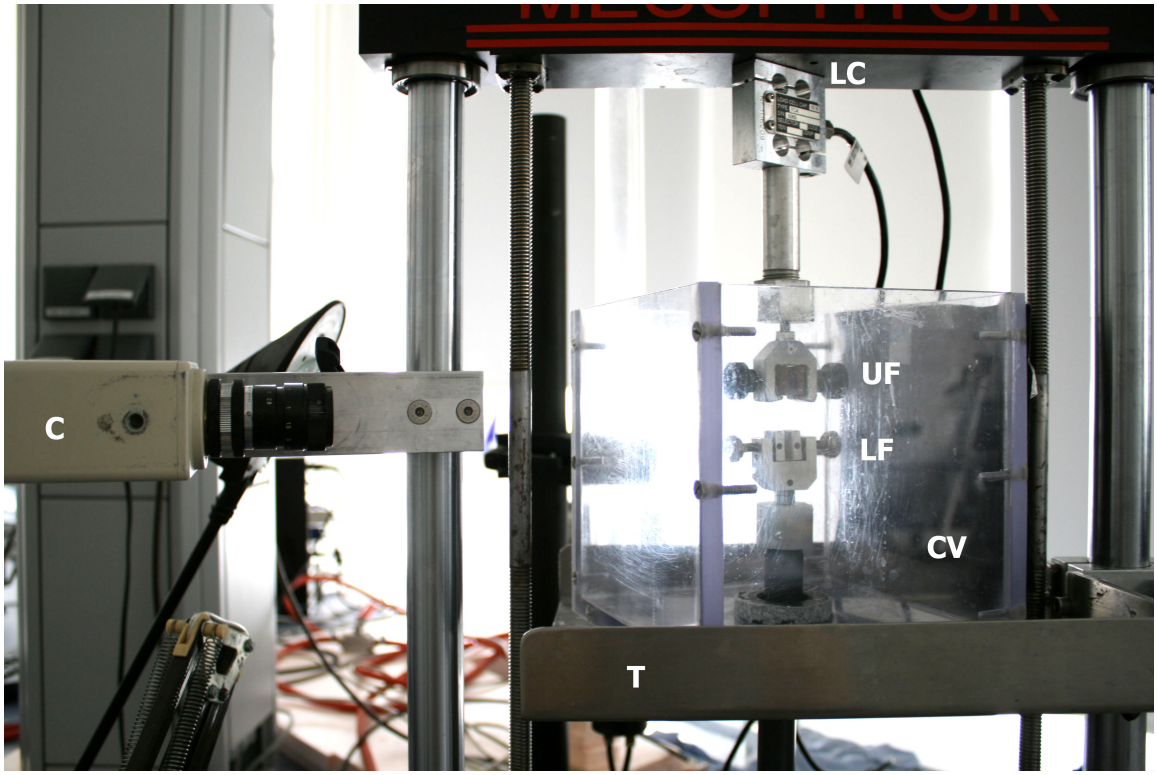

Figure 2.6: Detailed view of the experimental setup displaying the load cell (LC), cuvette (CV), CCD camera (C), upper fixing clamp (UF), lower fixing clamp (LF), metal table (T)

The load cell (Fig. 2.7) is a 10 N Class 1 strain-gauge load cell (type TCA 10 N, code CTCA1K5; AEP transducers, Modena, Italy) with a maximum loading capacity of 10 N and an accuracy of 0.03 % (Sommer et al., 2008).

The camera (Fig. 2.8) is a Mintron 1/3" CCD camera (Model: OS-65D (CCIR)) with a 50 mm objectiv and 3 baffle rings for the tensile tests. The technical data of the CCD camera are:

- horizontal resolution: 795 pixel
- vertical resolution: 596 pixel
- CCD chip: 8.5 $\times$ 6.4 mm
- minimum lighting: 0.5 lux at F1.2

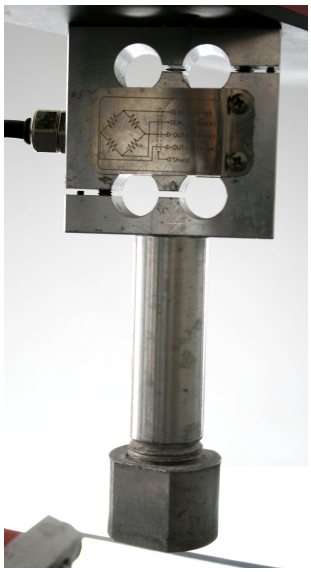

Figure 2.7: Detailed view of the load cell

Figure 2.8: Detailed view of the CCD camera

The heatbath (Fig. 2.9) is a Lauda Ecoline-Einhängethermostat E 200, which pumps the water through a heating coil to heat the tissue bath. The technical data of the E 200 are (Sommer, 2003):

- working temperature: $20 - 200\,^{\circ}\mathrm{C}$
- temperature stability: $\pm 0.01\,^{\circ}\mathrm{C}$
- heat capacity: 2.25 kW
- pump pressure: 0.4 bar
- delivery volume of the pump: max. 20 l/min

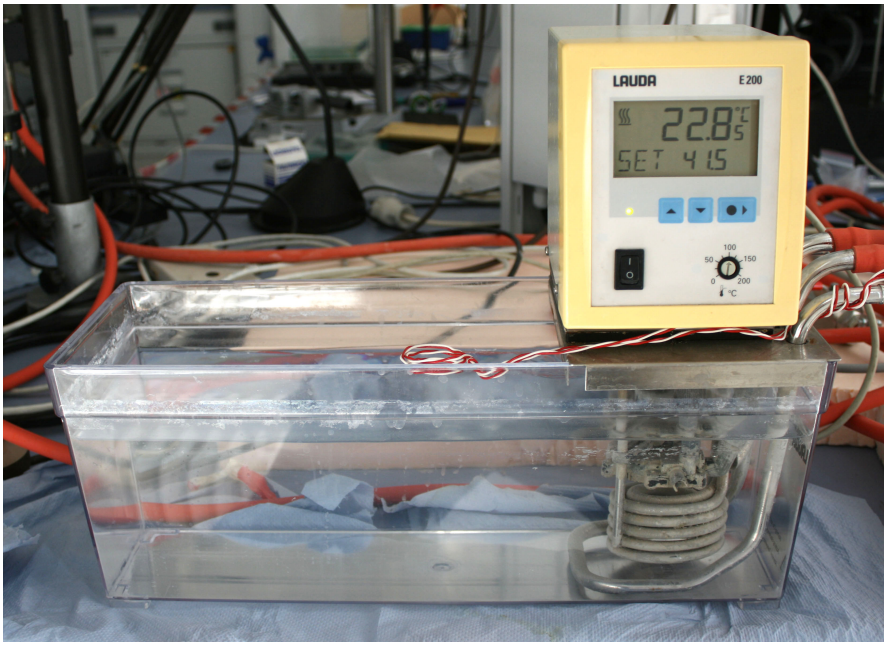

Figure 2.9: Heatbath

Figure 2.10 shows the computer which controlls the testing device by the EDC and collects the data of the CCD camera and the load cell. On the left monitor the measuring program is working and on the right monitor the videoextensometer program.

Figure 2.10: Computer with two monitors and running testsoftware

Figure 2.11 shows the two EDCs. The top one records the values from the load cell and the position of the crossbars and the lower one, which is only used during the inflation tests, records the pressure values from the pressure transducer and controlls the pump.

Figure 2.11: External Digital Controller for force (above) and pressure (below)

Extension-Inflation tests

The experimental setup for the inflation tests consists of the testing device, adjusted for the inflation tests, two external digital controllers, a pump with a reserve and a pressure cylinder, and a computer for recording the data of the EDCs and the videoextensometer (Fig. 2.12). For the inflation tests, another load cell and another sample holder tube on the upper crossbar and a pressure transducer on the lower crossbar are installed. The five-bar class 1 strain-gauge pressure transducer (model TP12, AEP transducers; Modena, Italy), which has an accuracy of 20 Pa, is connected via the pressure cylinder to the pump (model μ333, Neuhold, Graz, Austria), which pumps PBS from the reserve into the samples (Schulze-Bauer et al., 2002). The second EDC (Fig. 2.11) controlls the pump and the pressure transducer and transmits the data to the computer.

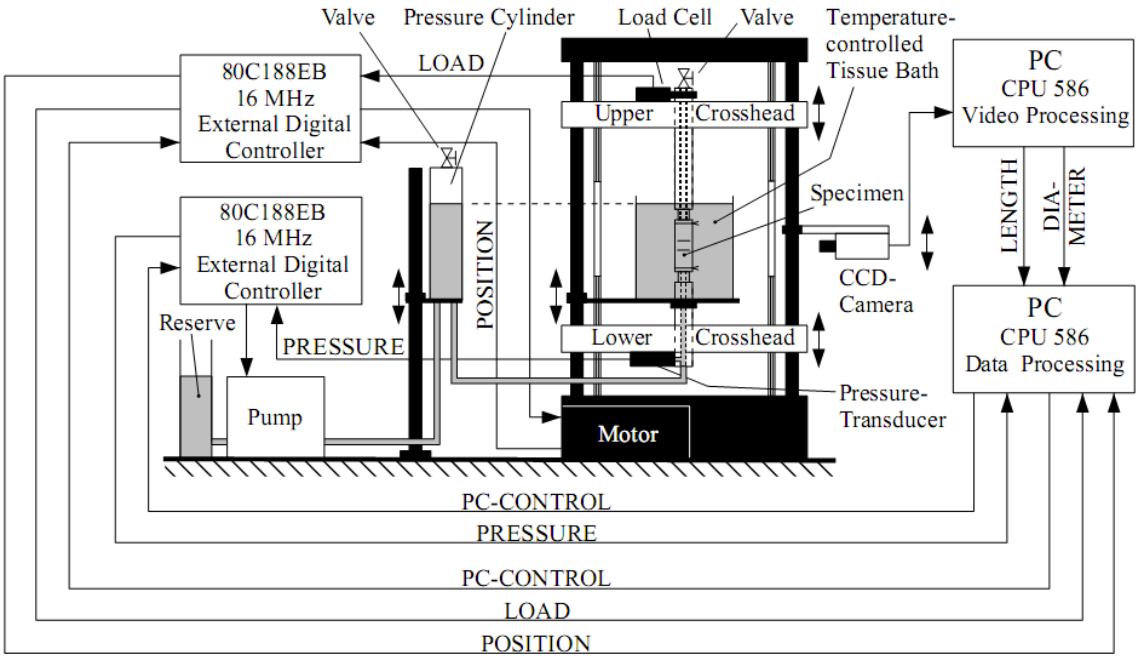

Figure 2.12: Schematic illustration of the inflation measuring equipment (adapted from Schulze-Bauer et al. (2002))

Figure 2.13 shows the actual strain instrument for the inflation tests. To ensure that the PBS, which is pumped into the sample, has the same temperature as the tissue bath, the reserve is placed in the heatbath. The CCD camera has been adjusted to the inflation tests with a 25 mm objectiv and only one baffle ring. The load cell is a bending load cell (model F1/1000N, AEP transducers; Modena, Italy) with a maximum capacity of 1 kN and an accuracy of 0.015 %.

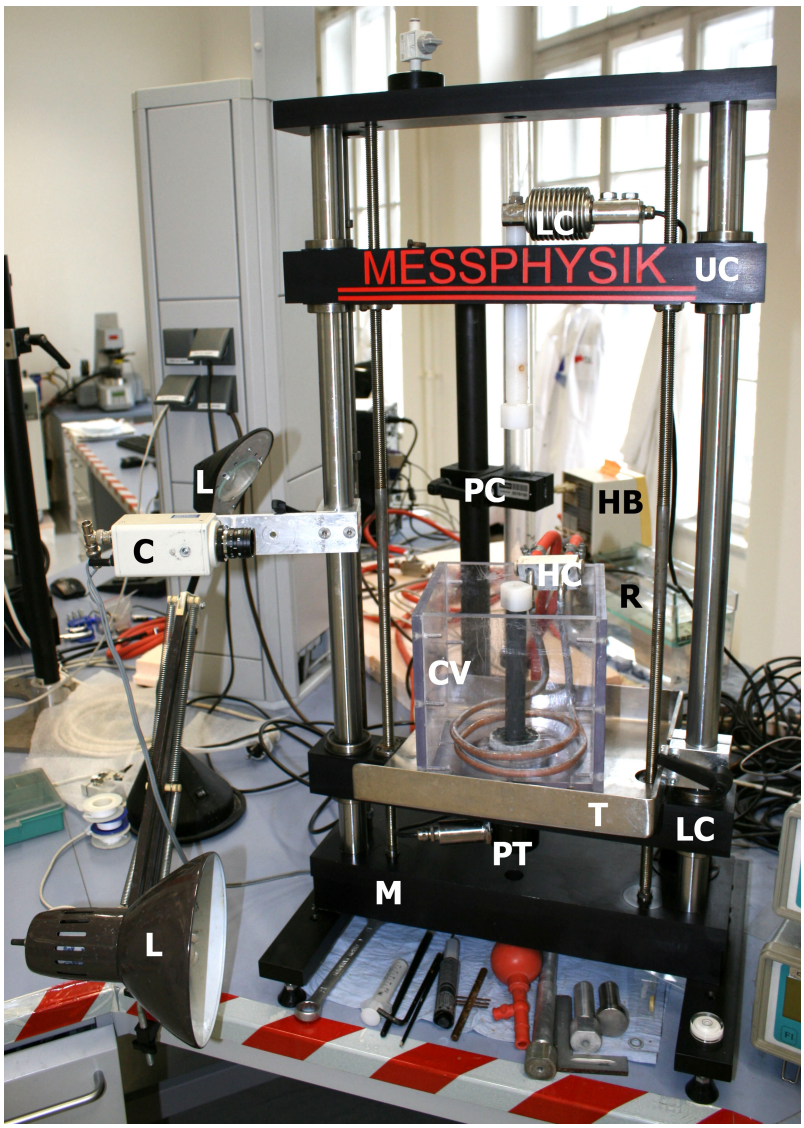

Figure 2.13: Experimental setup for inflation tests with LC: load cell, CV: cuvette, HC: heating coil, C: CCD camera, UC: upper crosshead, LC: lower crosshead, HB: heatbath, L: lamps, PT: pressure transducer, PC: pressure cylinder, R: reserve, M: motor, T: metal table

2.3.2 Testing software

The testing software consisted of two programs, the measuring program 'Kunststoffzugversuch, Version 2.10.01' and the videoextensometer program 'WinextNG, Version 5.26.0.0'. The measuring program controlled the testing device and the pump via the EDCs and recorded the data collected by the load cell and the pressure transducer. To perform the tests, a test protocol had to be written in the measuring program. The videoextensometer program recorded the picture from the CCD camera and measured the actual length and width of the samples. These values were than submitted to the measuring program.

Uniaxial tensile and rupture tests

The program raised the force on the sample five times from 0 N to the calculated force values, according to the test protocol in Chapter 2.4.1. After the last cycle, the program had to raise the force to 10 N to ensure the rupture of the samples.

Inflation tests

For the inflation tests the program looped the luminal pressure in the samples ten times between -0.6 and 2.65 kPa, according to the test protocol in Chapter 2.4.2. These values were needed, because the EDC regulated the pressure not very good, so the enhanced values in the program ensured the needed loops between 0 and 2 kPa.

2.4 Testing protocol

For every test a protocol had to be made, to guarantee a comparable result for all samples.

2.4.1 Uniaxial tensile and rupture tests

For these tests, the samples were subjected to five uniaxial loading-unloading cycles at a constant crossbar velocity of 10 mm/min and maximum first Piola Kirchhoff stress values of 12.5, 25, 50 and 100 kPa for the muscle samples and 25, 50, 100 and 200 kPa for the mucosa samples. The stress values for the muscle samples had to be half of the values for the mucosa samples, because the muscle showed a much smaller rupture strength and a higher thickness than the mucosa. The first four cycles were used for preconditioning and the fifth cycle was used for measurement (Figs. 2.14 and 2.15). The stress values had to be reconverted for the testing software to force values (N) with the measured thicknesses of the unloaded samples. After the overall twenty loading-unloading cycles, the stress was raised until the samples ruptured. For the ovine small intestine, the same test protocoll as for the mucosa of the esophagus was applied.

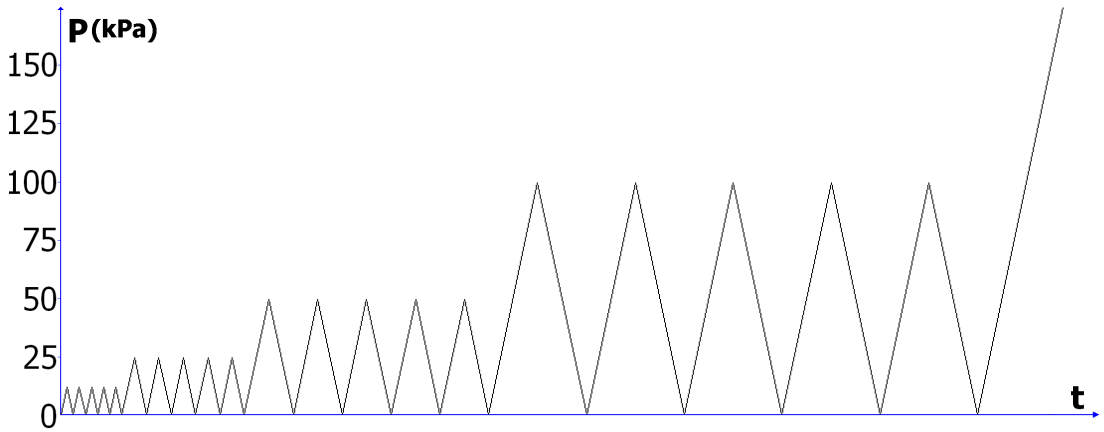

Figure 2.14: Testing protocol for the uniaxial tensile tests on muscle samples

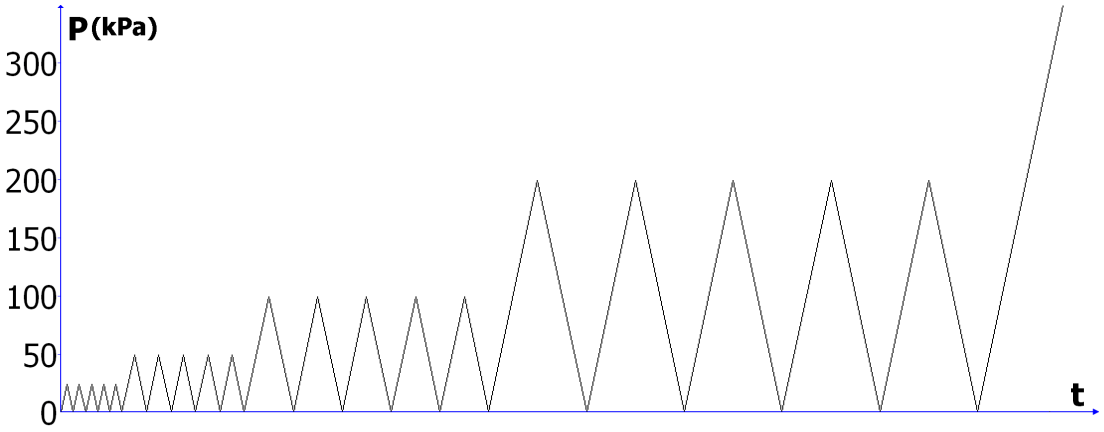

Figure 2.15: Testing protocol for the uniaxial tensile tests on mucosa samples

2.4.2 Inflation tests

For the inflation tests the samples were preconditioned 3 times from 0 to 10 % in the axial direction. Then a pressure in the range of 0-2 kPa was imposed and removed at a rate of 10 kPa/min for ten times to get the pressure-stretch data at the axial stretch ratio of 1.1. This protocol was repeated at axial stretch ratios of 1.2, 1.3 and 1.4. Figure 2.16 illustrates the whole time-dependance of the pressure and the axial stretch. The data of the last inflation at each extension level were used (Yang et al., 2006b). The inflation tests of the small intestine were obtained at 0 and 10 % axial pre-stretch at a pressure range from 0 to 1 kPa, also with ten loops.

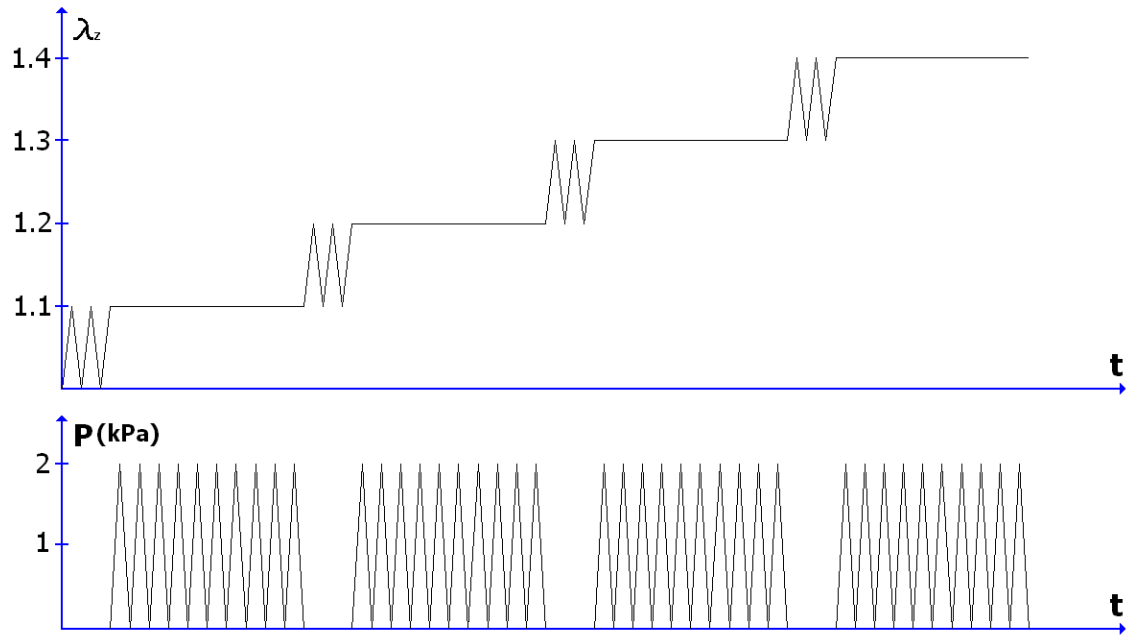

Figure 2.16: Testing protocol for the inflation tests

2.5 Experimental procedure

2.5.1 Sample preparation

Uniaxial tensile and rupture tests

For the uniaxial tests, the cleaned esophagus was cut to a piece of 8-9 cm length and sliced in axial direction with scissors. To distinct the axial from the circumferential direction during the whole preparation, a little cut was made at the upper end of the esophagus. The now flat esophagus had to be separated into the individual layers.
For this the mucosa-submucosa layer on top was cut off from the muscle layer below with scissors, which was relatively easy, because the submucosa was only loose connected to the muscle. Figure 2.17 shows the stages of the layer dissection.
After the separation, remains of connective and submucosa tissue were dissected from the two layers with scissors, to measure the mechanical behavior without the influence of other tissue than muscle or mucosa. Further investigations on how much of the submucosa tissue remains on the mucosa after dissection, and how this influences the mechanical properties of the tissue, have to be done.
With a punch cutter and a scalpel, two dog bone shaped samples, one in axial and one in circumferential direction, were prepared from each layer. Therefore, four individual samples were obtained from one esophagus. The punch cutter had an overall length of 38 mm, a grip-to-grip length of 20 mm and a gauge width of 4 mm.

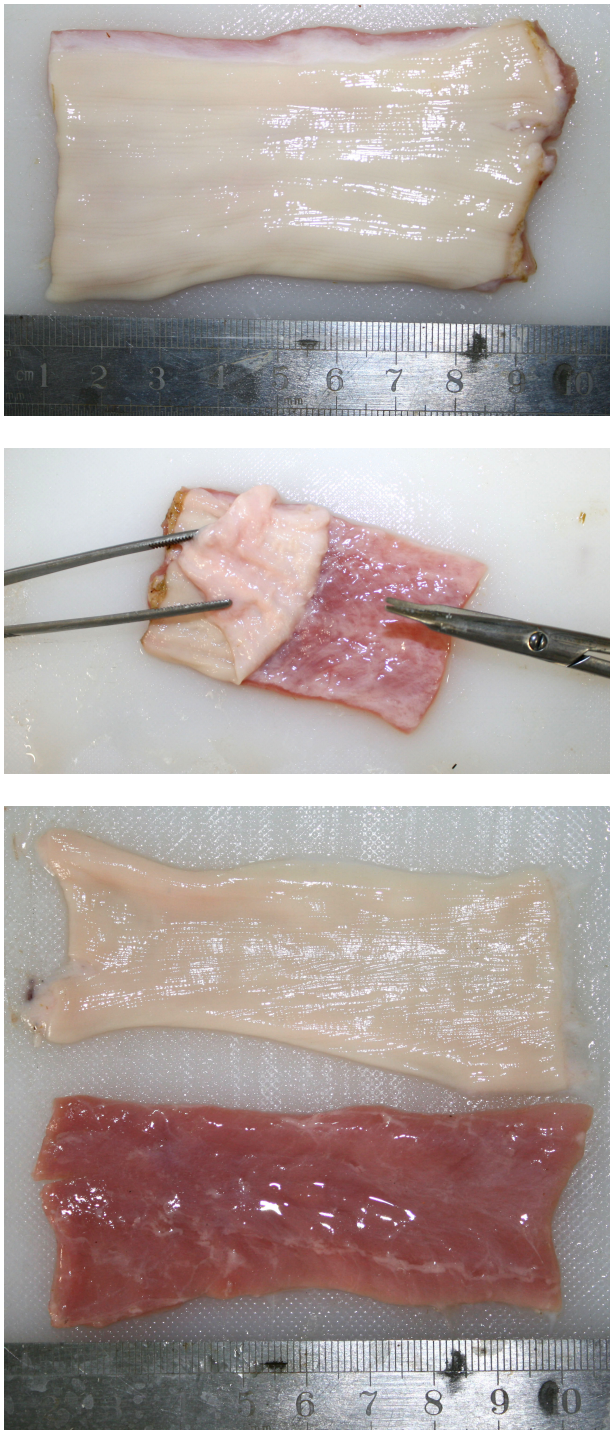

Figure 2.17: The stages of the layer dissection displaying the axially sliced esophagus (top), the separation of the muscle and mucosa layers (middle) and separated layers (bottom)

To prevent the samples from disengaging from the fixing clamps, abrasive paper strips were glued on the broad ends of the samples, with the abrasive side on the inside. For the length measurement, two small strips of ribbon, each one and a half millimeter long and a half millimeter wide, were glued on the middle of the samples with a distance of 4 mm from each other.
The sample preparation for the small intestine was the same as for the esophagus, but only two samples were prepared, because the layers of the intestine were not separated. Figure 2.18 show the prepared muscle and mucosa samples of the esophagus and the axial and circumferential samples of the small intestine.

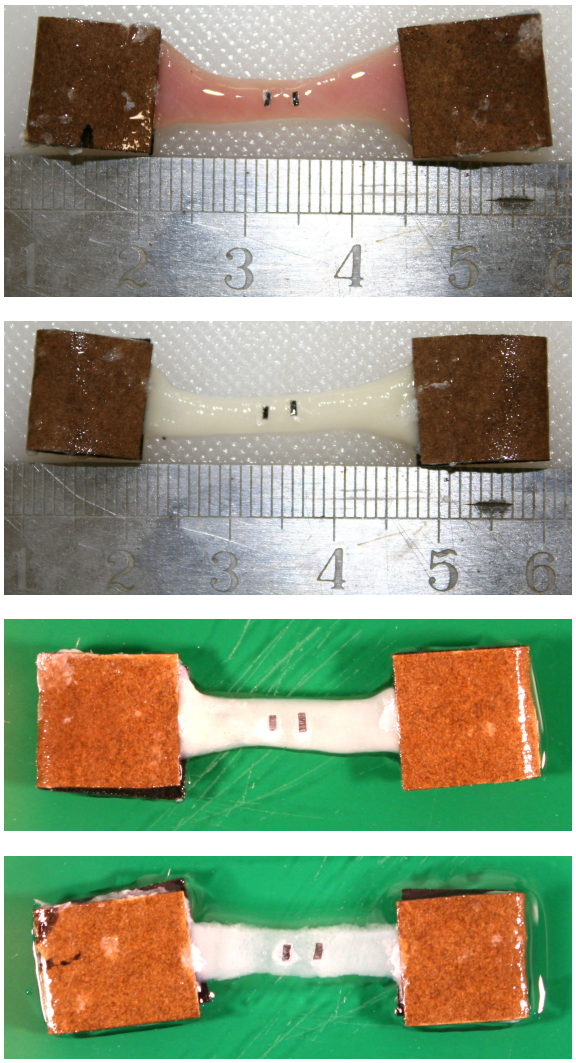

Figure 2.18: Prepared samples for the uniaxial tensile tests displaying the muscle sample of the esophagus (top), the mucosa sample of the esophagus (middle top), the small intestine sample in axial direstion (middle bottom) and the small intestine sample in circumferential direction (bottom)

Inflation tests

Like for the tensile tests, the cleaned esophagus was shortened to a length of 8-9 cm. To fit the esophagus into the experimental setup, two canulas with screw threads were glued into the ends of the sample. The canulas were aditionally fixed with a thin cord. To measure the elongation of the sample, two small strips of ribbon, each with a length of 3 mm and a width of 1 mm, were glued on the middle of the sample with a distance of 1 cm from each other (Fig. 2.19).
An intestine sample was also prepared for the inflation tests. The procedure was the same as for the esophagus. Figure 2.20 shows the prepared sample.

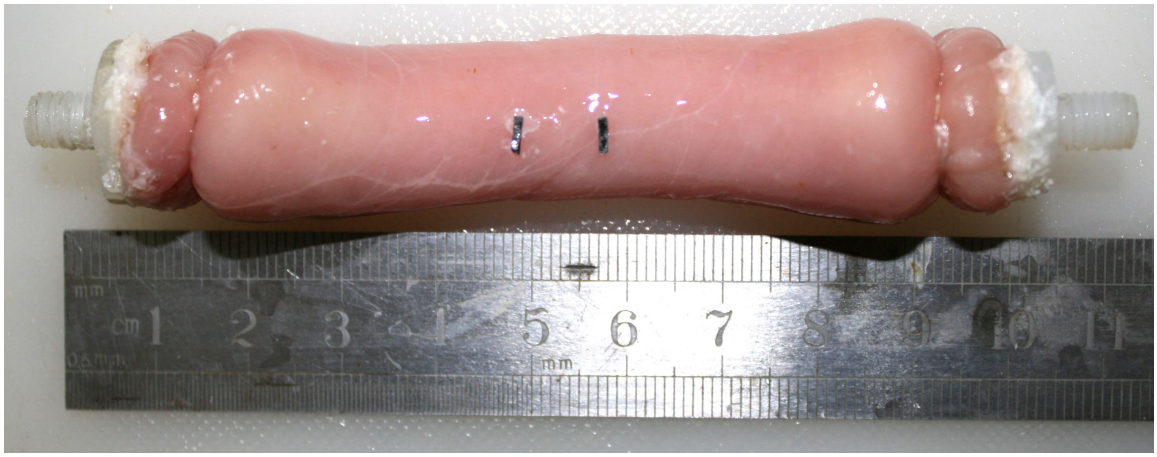

Figure 2.19: Esophagus after attaching the markers

Figure 2.20: Prepared intestine sample for the inflation tests

2.5.2 Experimental preparations

Tensile and rupture tests

Before the measurements, the experimental setup had to be prepared. First the cuvette was mounted on the lower sample holder tube and the lower fixing clamp was screwed on. Then the heating coil and the digital thermometer were put into the cuvette. Three liters of PBS and 300 mg EGTA were filled in the cuvette and the heatbath was turned on to heat the tissue bath to $37\,^{\circ}\mathrm{C}$, which took approximately one hour. Then the upper fixing clamp was screwed on the load cell and both fixing clamps were adjusted parallel to the camera.

The camera settings for the tensile and rupture tests were:

- 50 mm objectiv
- aperture 8
- 3 baffle rings
- camera position 1
- measurement with waterfilled cuvette
- parameter setting: 000_Zugversuch.par

During the heating of the tissue bath, the computer and the EDC were started. As soon as the EDC was ready by displaying the status message PC-CONTROL, the measurement programm and the videoextensometer programm could be started.

Inflation tests

The preparations for the inflation tests were similar to those for the tensile tests with some important differences. The load cell had to be replaced by a model attached on the upside of the crossbar and a sample holder tube with a valve had to be fixed on the new load cell. The fixing clamps had to be removed, because the inflation samples were fixed with the canulas, not with the fixing clamps. Since the axial force and the pressure had to be measured, both EDCs had to be used. For the saline to be pumped into the samples, the reserve tank was filled with 1.5 l of PBS and 150 mg EGTA and put into the heat bath to heat it up to $37\,^{\circ}\mathrm{C}$. The reserve was then connected to the pump, which pumped the PBS during the tests into the pressure cylinder and from there into the sample.

The camera settings for the inflation tests were:

- 25 mm Objektiv
- aperture 8
- 1 baffle ring
- camera position 3
- measurement with waterfilled cuvette
- parameter setting: Tube_25mm_Blende8.par

Thickness measurements

For these measurements the lower fixing clamp had to be screwed on the sample holder tube and a microscopic slide with a plastic handle had to be positioned on the clamp. The edge of the microscopic slide facing the camera was colored with a black textmarker, and a sheet of white paper was put behind the microscopic slide to improve the contrast between the sample and the background to ensure an accurate measurement of the thickness.

The camera settings for the Thickness measurings were:

- 50 mm objectiv
- aperture 8
- 3 baffle rings
- camera position 3
- measurement without waterfilled cuvette
- parameter setting: 00_Dickenmessung.par

2.5.3 Calibration of the videoextensometer

The calibration of the camera had to be done with a calibration standard before every measurement. The calibration standard had to be fixed in the lower fixing clamp and the camera had to be focused on the three crossbars of the standard. Two lamps and a sheet of white paper behind the calibration standard were used to adjust the contrast.
The settings for the measuring axis were set to 'black on white' for the longitudinal axis and to 'black object' for the cross axis. For the calibration of the longitudinal axis, the distance between the two outer crossbars (11 mm) was measured and for the calibration of the cross axis the width of the calibration standard (8 mm) was measured.
For the thickness measurements, only the longitudinal axis was calibrated with the camera settings listed in Chapter 2.5.2: Thickness measurements.
For the uniaxial tensile and rupture tests, the axis were calibrated with the camera settings listed in Chapter 2.5.2: Tensile and rupture tests. With these settings the field of sight was 20×15 mm.
For the inflation tests, the axis were calibrated with the camera settings listed at Chapter 2.5.2: Inflation tests. With these settings the field of sight was 44×33 mm.

2.5.4 Thickness measurements

To measure the uniaxial stress-stretch behavior of the muscle and mucosa samples, the thickness of the unloaded samples had to be determined first. For this, the sample was laid onto the microscope slide, so that the long side of the sample facing the camera was flush to the colored edge of the microscopic slide. The setting for the measuring axis was set to 'black object', and the lighting was adjusted to get a high contrast between the dark sample and the white background. Now the thickness of the sample could be measured, without the tissue bath, twice on every long side of the sample. The thickness of the microscopic slide (1 mm) had to be subtracted from the result, because slide and sample were measured together. The mean value of the four measured thickness values was used to calculate the force values for the uniaxial tensile and rupture tests.

2.5.5 Tensile and rupture tests

For this test, the sample was fixed in the upper fixing clamp and the crossheads were closed until the sample was at the same height as the lower fixing clamp. Then the tissue bath was raised to offset the weight of the sample and the values of force and path in the measuring program were tared. Then the tissue bath was lowered, the sample was fixed in the lower fixing clamp, and the tissue bath was raised again, until the measured force was zero, and fixed with the metal table. For an optimal alignment the camera had to be focused on the markers of the sample and the front side of the cuvette had to be normal to the camera. The contrast was adjusted with two lamps and a sheet of black paper behind the cuvette. After setting the measuring axis to 'black on white' for the longitudinal axis and to 'white object' for the cross axis, the videoextensometer could be started in both programs. Then

the test protocol was adjusted to the thickness of the sample by filling in the calculated force values, and then a new test could be started.

2.5.6 Inflation tests

For measuring the inflation behavior of the esophagi, the tube samples were screwed in with the canula in the upper sample holder tube and the crossbars were closed until the sample was at the same height as the lower sample holder tube. Then the tissue bath was raised to tare the force and path values. After lowering the tissue bath, the sample had to be carefully screwed in the lower sample holder tube without twisting it. Then the sample was adjusted, so that the markers were facing the camera, and the tissue bath was raised and fixed with the metal table.
The pressure in the sample was raised until PBS came out of the valve above the sample. Then the pressure was lowered a little bit, the valve was closed and the pressure was further lowered until the water levels in the tissue bath and in the pressure cylinder were the same. After taring the pressure, the pressure cylinder was closed with the valve on the top and the pressure value was lowered to zero.
The contrast was then adjusted with two lamps and a sheet of black paper behind the cuvette. Like for the tensile tests, the measuring axis were set to 'black on white' for the longitudinal axis and to 'white object' for the cross axis, and the videoextensometer could be started in both programs. Since the test protocol had no sample specific values, a new test could be started immediately.

2.5.7 Calculation of the Cauchy stress σ

The Cauchy stress σ had to be calculated from the measured data as followed:

$$\sigma = \frac{f}{a} = \frac{f}{wt} = \frac{fl}{V} = \frac{f\lambda}{WT}, \tag{2.1}$$

with

$$V = LWT = lwt = const. \Longrightarrow t = \frac{V}{lw} \tag{2.2}$$

and

$$\lambda = \frac{l}{L} \tag{2.3}$$

Here, f is the force in the actual configuration, a the area in the actual configuration and V the volume in both the actual and the reference configuration. L, W and T are length, width and thickness of the sample in the reference configuration, and l, w, and t are length, width and thickness in the actual configuration (Sommer, 2003).

3 Results

3.1 Thickness measurements

The Tables 3.1 and 3.2 show the results of the thickness measurements for the uniaxial tensile and rupture tests. As can be seen by the mean values of the results, the mucosa is around 1 mm thinner than the muscle and the samples have nearly the same thickness in axial and circumferential directions.

Table 3.1: Results of the unloaded thickness measurements (muscle samples)

Sample number	Muscle axial (mm)	Muscle circumferential (mm)
1	1.53	—
3	1.90	2.19
4	2.52	2.82
5	1.56	1.90
6	2.48	2.60
7	2.86	2.91
8	2.54	2.65
9	1.86	2.21
10	2.27	2.54
11	1.96	2.19
12	1.83	2.51
Mean $\pm$ SD	2.13 ± 0.43	2.45 ± 0.32

Table 3.2: Results of the unloaded thickness measurements (mucosa samples)

Sample number	Mucosa axial (mm)	Mucosa circumferential (mm)
1	1.60	1.61
2	1.68	1.53
3	1.25	1.34
4	1.16	1.34
5	1.00	1.21
6	1.18	1.10
7	1.32	1.48
8	1.20	0.84
9	1.09	1.02
11	1.01	0.82
12	1.10	0.82
Mean $\pm$ SD	1.24 ± 0.22	1.19 ± 0.29

The thicknesses of the two intestine samples were: 0.77 mm for the sample in axial direction and 0.69 mm for the sample in circumferential direction.

3.2 Uniaxial tensile tests

For these tests, the last cycle of each of the four series, obtained at 12.5, 25, 50 and 100 kPa for the muscle samples and at 25, 50, 100 and 200 kPa for the mucosa samples, were taken for measurement. In the Figs. 3.1 - 3.4 the Cauchy stress σ is plotted as a function of the stretch λ. To compare the results of all sample the stretch values of the highest stress values were measured.
Both layers showed anisotropic and nonlinear behavior. The heterogeneity of the esophagus was more distinctive in axial than in circumferential direction. The hysteresis of both layers was smaller in axial than in circumferential direction.
The muscle samples in axial direction showed the highest stiffness, and the lowest Cauchy stress values, compared to the other layers and directions. The mean values of the muscle samples in axial direction, shown in Figure 3.1, are listed in Table 3.3.
In circumferential direction, the muscle layer showed a high extensibility at all four stress levels, which reached almost 100 %, and much higher Cauchy stress values than in axial direction. The mean values of the muscle samples in circumferential direction, shown in Figure 3.2, are listed in Table 3.4.
The stiffness of the mucosa in axial direction was higher than that in circumferential direction, but lower than the stiffness of the muscle layer in the axial direction. The mean values of the mucosa samples in axial direction, shown in Figure 3.3, are listed in Table 3.5.

In circumferential direction, the mucosa was much softer than in axial direction, but was always stiffer than the muscle in circumferential direction, and the Cauchy stress values were also higher than in axial direction. The mean values of the mucosa layer in circumferential direction, shown in Figure 3.4, are listed in Table 3.6.
The results for the intestine samples show, that in the first two cycles, the circumferential direction is stiffer than the axial direction, while in the following cycle the axial direction is stiffer, but not very much. A fourth cycle of the circumferential direction could not be obtained, because the sample ruptured already at 273 kPa. The values of the intestine samples, shown in Figs. 3.5 and 3.6, are listed in Table 3.7.

Table 3.3: Mean values and standard deviations of the stretch λ and the Cauchy stress σ for the muscle samples in axial direction of the uniaxial tensile tests, depending on the maximum first Piola-Kirchhoff stress values.

1st PK stress P (kPa)	Stretch λ (-)	Cauchy stress σ (kPa)
12.5	1.10 ± 0.05	15.9 ± 3.3
25	1.13 ± 0.06	32.0 ± 6.7
50	1.17 ± 0.08	65.4 ± 13.5
100	1.23 ± 0.12	136 ± 28

Table 3.4: Mean values and standard deviations of the stretch λ and the Cauchy stress σ for the muscle samples in circumferential direction of the uniaxial tensile tests, depending on the maximum first Piola-Kirchhoff stress values.

1st PK stress P (kPa)	Stretch λ (-)	Cauchy stress σ (kPa)
12.5	1.24 ± 0.09	18.9 ± 3.7
25	1.47 ± 0.16	42.9 ± 8.1
50	1.69 ± 0.27	99.2 ± 15.6
100	1.88 ± 0.40	216 ± 30

Table 3.5: Mean values and standard deviations of the stretch λ and the Cauchy stress σ for the mucosa samples in axial direction of the uniaxial tensile tests, depending on the maximum first Piola-Kirchhoff stress values.

1st PK stress P (kPa)	Stretch λ (-)	Cauchy stress σ (kPa)
25	1.22 ± 0.07	42.9 ± 7.6
50	1.30 ± 0.12	92.9 ± 17.8
100	1.37 ± 0.16	196 ± 41
200	1.43 ± 0.19	396 ± 83

Table 3.6: Mean values and standard deviations of the stretch λ and the Cauchy stress σ for the mucosa samples in circumferential direction of the uniaxial tensile tests, depending on the maximum first Piola-Kirchhoff stress values.

1st PK stress P (kPa)	Stretch λ (-)	Cauchy stress σ (kPa)
25	1.34 ± 0.11	43.3 ± 9.0
50	1.48 ± 0.12	95.4 ± 17.4
100	1.61 ± 0.14	208 ± 39
200	1.77 ± 0.18	462 ± 97

Table 3.7: Maximum stretch λ and Cauchy stress σ of the small intestine tensile tests, depending on the maximum first Piola-Kirchhoff stress values.

1st PK stress P (kPa)	Stretch λ (-)	Cauchy stress σ (kPa)
25 axial	1.12	33.8
25 circ.	1.06	35.2
50 axial	1.17	71.4
50 circ.	1.14	84.3
100 axial	1.21	144
100 circ.	1.22	185
200 axial	1.25	295

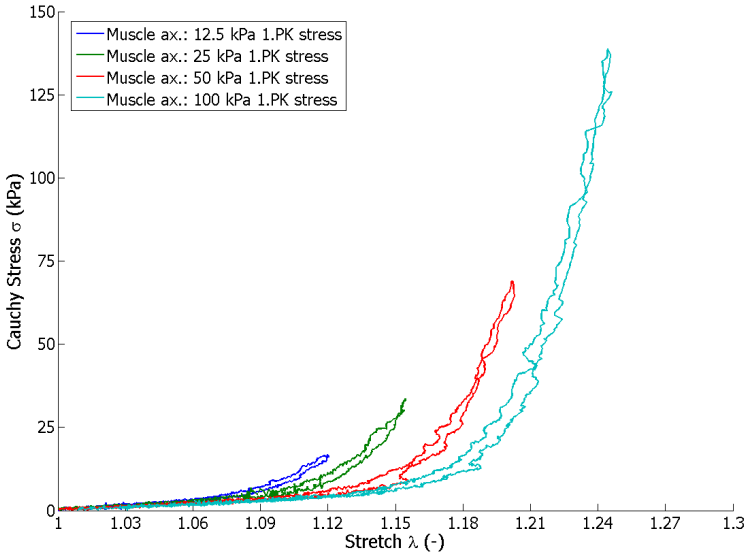

Figure 3.1: Representative results of the stretch λ and the Cauchy stress σ for the muscle samples in axial direction of the uniaxial tensile tests with maximum first Piola-Kirchhoff stress values of 12.5, 25, 50 and 100 kPa

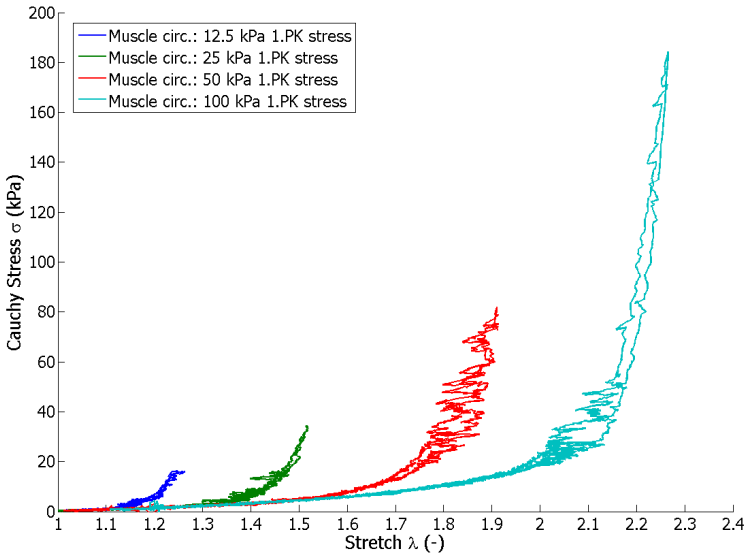

Figure 3.2: Representative results of the stretch λ and the Cauchy stress σ for the muscle samples in circumferential direction of the uniaxial tensile tests with maximum first Piola-Kirchhoff stress values of 12.5, 25, 50 and 100 kPa

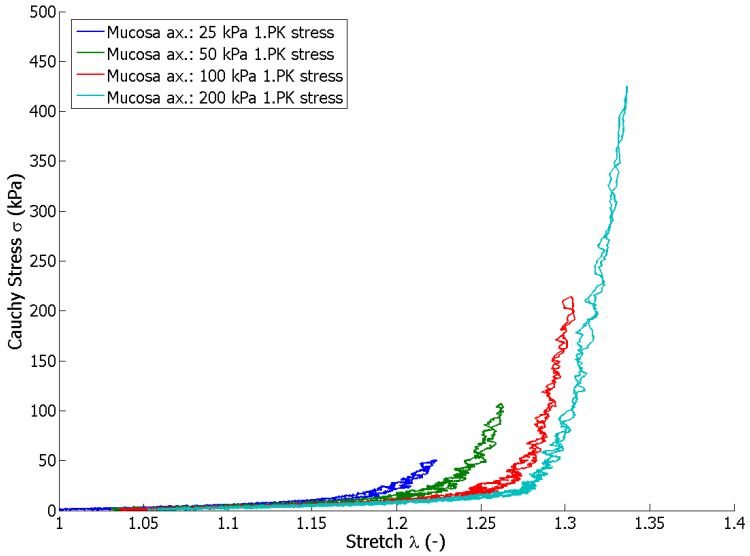

Figure 3.3: Representative results of the stretch λ and the Cauchy stress σ for the mucosa samples in axial direction of the uniaxial tensile tests with maximum first Piola-Kirchhoff stress values of 25, 50, 100 and 200 kPa

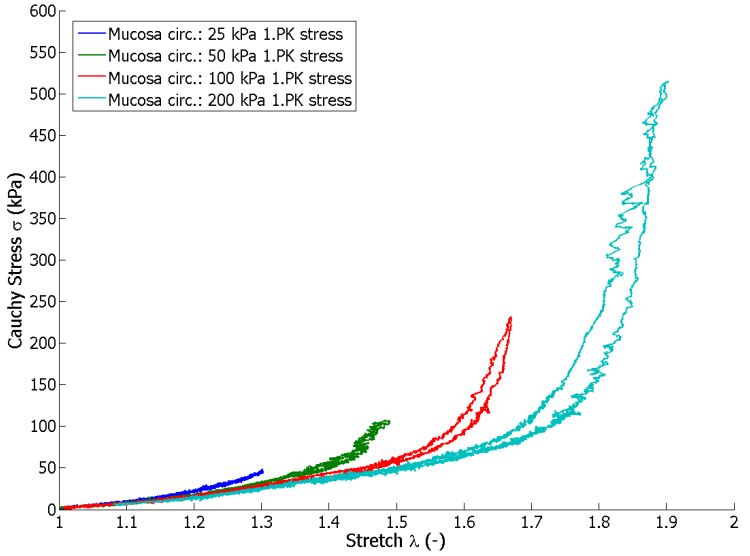

Figure 3.4: Representative results of the stretch λ and the Cauchy stress σ for the mucosa samples in circumferential direction of the uniaxial tensile tests with maximum first Piola-Kirchhoff stress values of 25, 50, 100 and 200 kPa

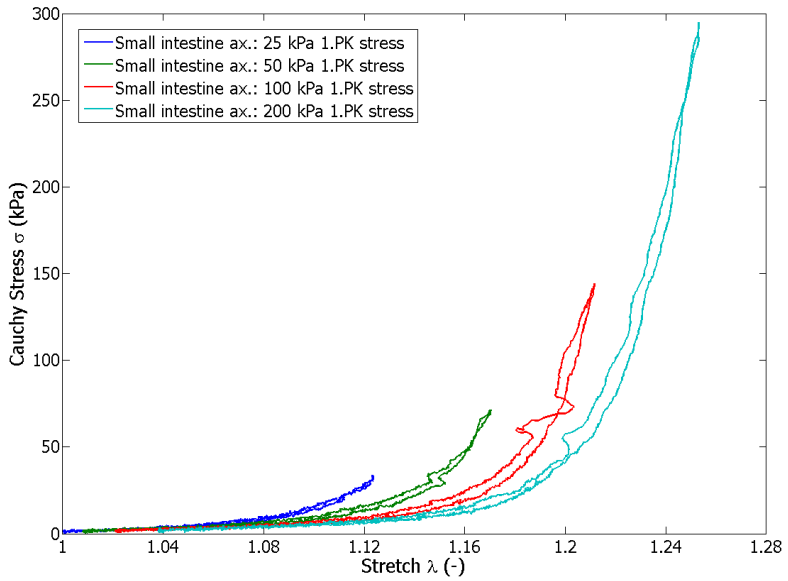

Figure 3.5: Results of the uniaxial tensile tests of the intestine sample in axial direction with maximum first Piola-Kirchhoff stress values of 25, 50, 100 and 200 kPa

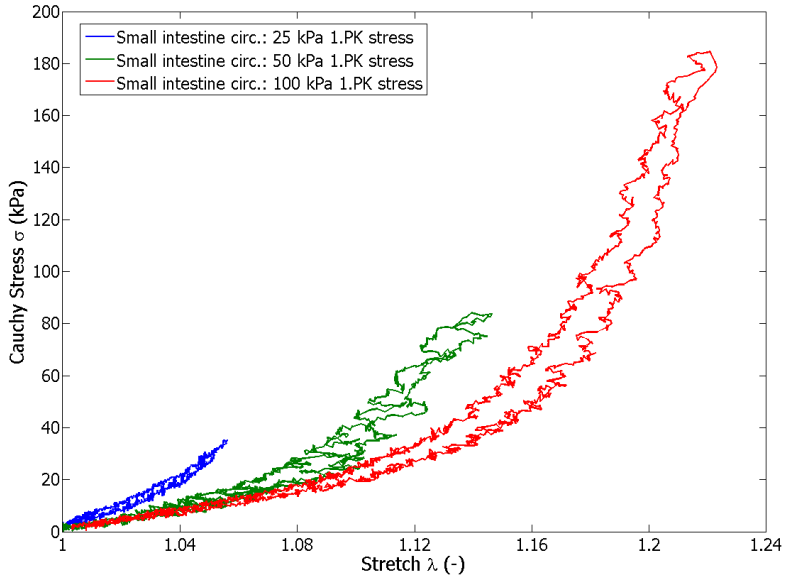

Figure 3.6: Results of the uniaxial tensile tests of the intestine sample in circumferential direction with maximum first Piola-Kirchhoff stress values of 25, 50, 100 and 200 kPa

3.3 Uniaxial rupture tests

The results of the rupture tests, given as the maximum Cauchy stress σ, depending on the stretch λ, and shown in Tables 3.8 and 3.9 and in Figure 3.7, indicated a high difference between the rupture strength of the two layers. The mucosa samples were much more resistant than the muscle samples, and both layers were more resistant in the axial direction than in the circumferential direction.
The values of the rupture strength of the small intestine samples, shown in Figure 3.8 were 1015 kPa in axial direction and 273 kPa in circumferential direction.

Table 3.8: Results of the uniaxial rupture strength of the muscle samples in terms of the Cauchy stress σ

Sample number	Muscle axial (kPa)	Muscle circumferential (kPa)
3	435	551
4	628	416
5	1401	1137
6	1107	502
7	426	753
8	563	403
9	696	620
10	714	932
11	547	399
12	780	592
Mean $\pm$ SD	730 ± 307	630 ± 245

Table 3.9: Results of the uniaxial rupture strength of the mucosa samples in terms of the Cauchy stress σ

Sample number	Mucosa axial (kPa)	Mucosa circumferential (kPa)
1	1201	486
2	933	—
3	2175	1315
4	3359	1192
5	2886	785
6	2858	2202
7	3029	1393
8	2451	1158
9	2815	1754
11	1887	2353
12	4521	2731
Mean $\pm$ SD	2556 ± 1004	1537 ± 714

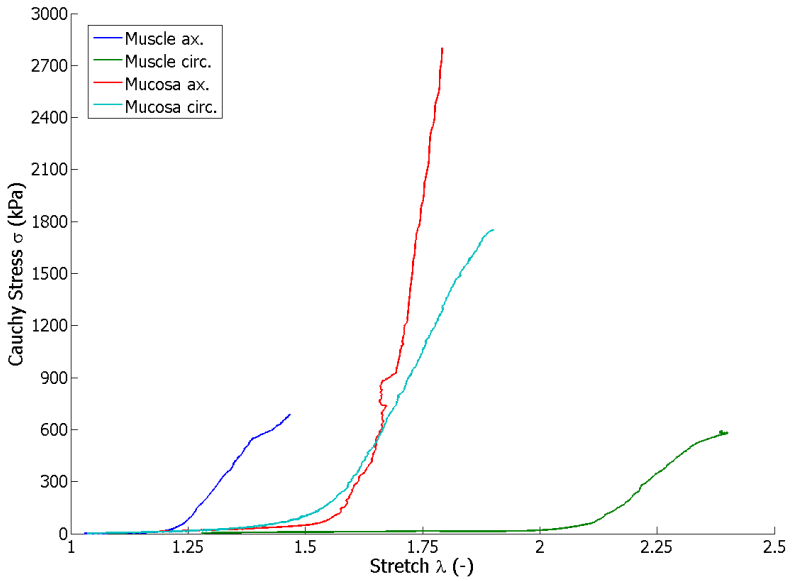

Figure 3.7: Representative results of the rupture strength of the muscle and the mucosa in axial and circumferential direction

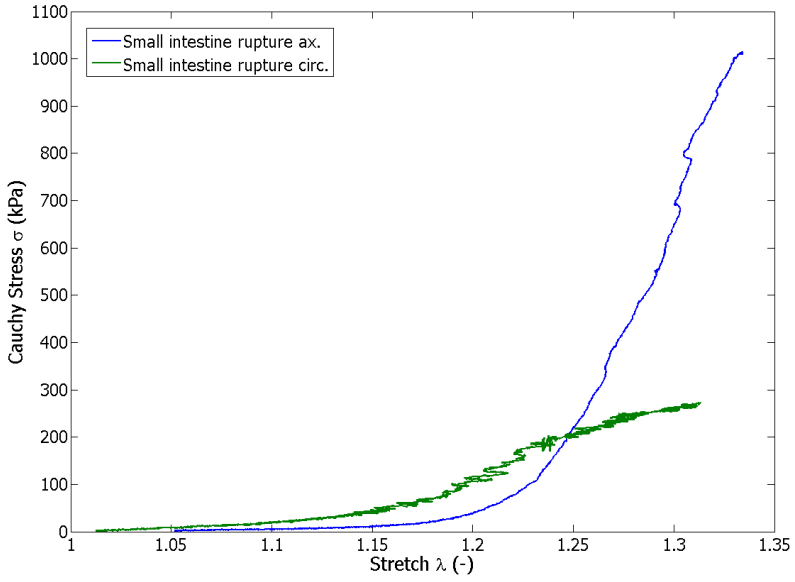

Figure 3.8: Results of the rupture strength of the small intestine in axial and circumferential direction

3.4 Inflation tests

During the inflation tests, the circumferential stretch λ_c and the axial stretch λ_z of the tube shaped esophagus samples had to be determined as a function of the pressure inside the samples. Four series were measured with an axial pre-stretch of 10, 20, 30 and 40 %. Like in the tensile tests, the last cycle of every series was used for measurement. All four series showed a high standard deviation, which made it difficult to interpret the results, but it was obvious, that the esophagi showed a strong softening in circumferential direction during the series, which reached its maximum at a pre-stretch level of 30 % (Fig. 3.9). With higher levels of pre-stretch the samples become stiffer. The axial stretch λ_z of the samples showed also a slight increase during the test with a much smaller standard deviation than λ_c, which additionally decreased strongly with higher axial pre-stretch (Fig. 3.10). Table 3.10 shows the mean values and the standard deviation of λ_c and λ_z for all four series.

Table 3.10: Results of the circumferential and the axial stretch of the inflation tests, depending on the axial pre-stretch

axial pre-stretch (%)	circumferential Stretch λ_c (-)	axial Stretch λ_z (-)
10	1.53 ± 0.14	1.17 ± 0.12
20	1.51 ± 0.23	1.21 ± 0.06
30	1.57 ± 0.19	1.33 ± 0.05
40	1.56 ± 0.19	1.40 ± 0.01

The results of the intestine inflation tests (Table: 3.11 and Figs. 3.11 and 3.12) show a circumferential stretch of nearly 50 % at 0 % pre-stretch and nearly 40 % at 10 % pre-stretch and an axial stretch of 6 and 12 % at 0 and 10 % pre-stretch respectively.

Table 3.11: Results of the circumferential and the axial stretch of the inflation tests of small intestine samples, depending on the axial pre-stretch

axial pre-stretch (%)	circumferential Stretch λ_c (-)	axial Stretch λ_z (-)
0	1.51	1.06
10	1.39	1.12

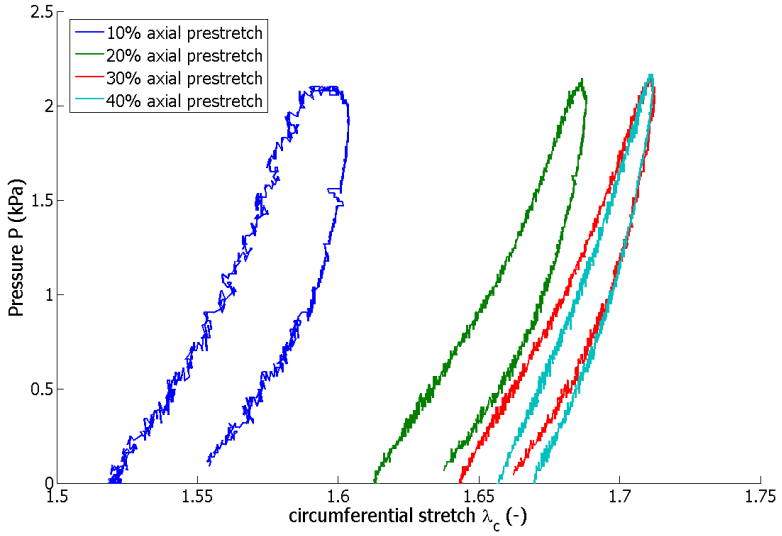

Figure 3.9: Representative results of the circumferential stretch for the inflation tests at axial pre-stretches ranging from 10 to 40 %

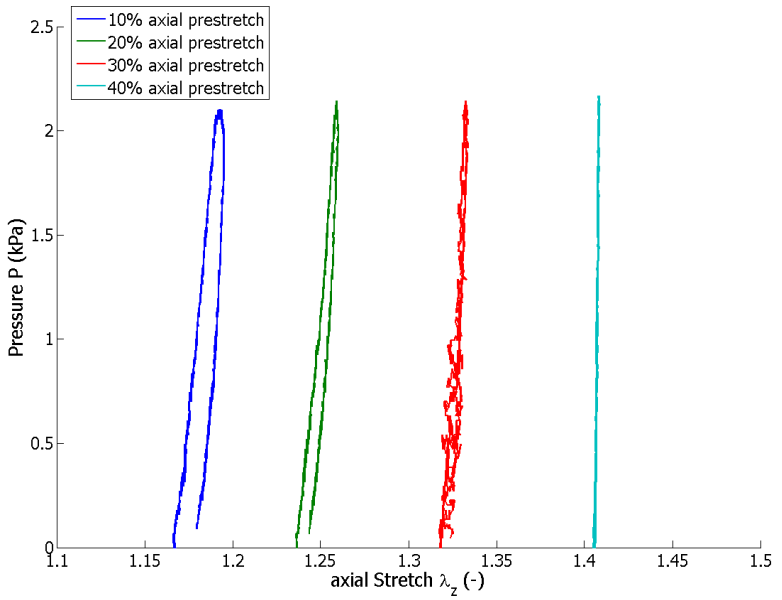

Figure 3.10: Representative results of the axial stretch for the inflation tests at axial pre-stretches ranging from 10 to 40 %

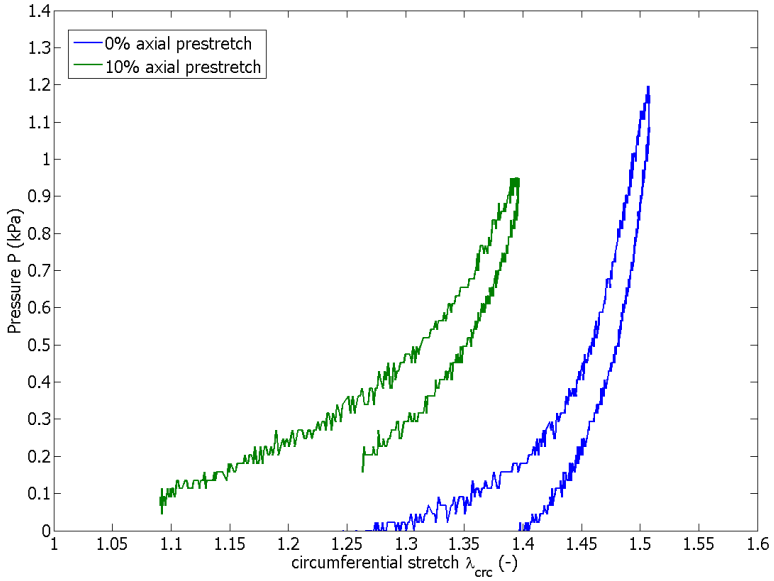

Figure 3.11: Results of the circumferential stretch for the inflation tests on small intestine samples at axial pre-stretches of 0 and 10 %

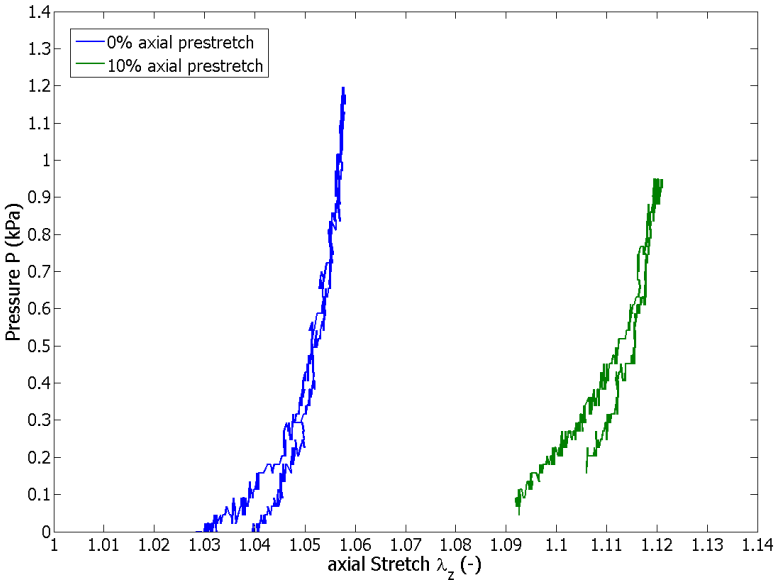

Figure 3.12: Results of the axial stretch for the inflation tests on small intestine samples at axial pre-stretches of 0 and 10 %

4 Discussion

4.1 Results

4.1.1 Thickness

Tables 3.1 and 3.2 show the results of the thickness measurements for the uniaxial tensile and rupture tests. The mean values with the standard deviation are

- 2.13 ± 0.43 mm for the muscle layer in axial direction
- 2.45 ± 0.32 mm for the muscle layer in circumferential direction
- 1.24 ± 0.22 mm for the mucosa layer in axial direction
- 1.19 ± 0.29 mm for the mucosa layer in circumferential direction.

The thickness ratio of muscle to mucosa is 1.72:1 in axial direction and 2.06:1 in circumferential direction.
The thickness values of the small intestine samples were 0.77 mm in axial direction and 0.69 mm in circumferential direction.

Natali et al. (2009) have found mean thickness values for porcine esophagi of 2 mm for the submucosa-mucosa layer and 3 mm for the muscle layer. The same values were obtained from Yang et al. (2006a), also for porcine esophagi. The only found values for sheep esophagi were obtained by Floyd and Morrison (1974), but they only measured the thickness of the muscle. With a value of 1.5 mm the muscle was thinner than the results found here. For the whole porcine esophagus, Yang et al. (2006c) found a mean thickness of 3-4 mm. Sokolis (2010) found for rabbit esophagi, that the mucosa-submucosa was two and three times thinner than muscle and intact esophagus, respectively.

A similar thickness ratio of the tissue engineered esophagi would be desirable for a better comparison of the biomechanical behavior between the ovine and the tissue engineered esophagi. At the moment, tissue engineered esophagi show a thickness of 4 mm, which is way too high, especially as this constructs consist only of epithelial cells and have no additional muscle layer (Saxena et al., 2010).

4.1.2 Tensile tests

The results for the uniaxial tensile tests are shown in Table 3.3 and Figure 3.1 for the muscle samples in axial direction, Table 3.4 and Figure 3.2 for the muscle samples in circumferential direction, Table 3.5 and Figure 3.3 for the mucosa samples in axial direction and Table 3.6 and Figure 3.4 for the mucosa samples in circumferential direction. Table 3.7 and Figs. 3.5 and 3.6 show the results for the uniaxial tensile tests of the small intestine samples.
Both layers showed anisotropic and nonlinear behavior. The heterogeneity of the esophagus was more distinctive in axial than in circumferential direction. The hysteresis of both layers was smaller in axial than in circumferential direction.
The muscle samples showed in axial direction the highest stiffness and the lowest Cauchy stress values. In circumferential direction, the muscle layer showed a high extensibility at all four stress levels, which reached almost 100 %, and much higher Cauchy stress values than in axial direction. The stiffness of the mucosa in axial direction was higher than that in circumferential direction, but lower than the stiffness of the muscle layer in the axial direction. In circumferential direction, the mucosa was much softer than in axial direction, but was always stiffer than the muscle in circumferential direction, and the Cauchy stress values were also higher than in axial direction.
The results for the intestine samples show, that in the first two cycles, the circumferential direction is stiffer than the axial direction, while in the following cycle the axial direction is stiffer, but not very much. A fourth cycle of the circumferential direction could not be obtained, because the sample ruptured already at 273 kPa.

Natali et al. (2009) and Yang et al. (2006a) obtained similar results for porcine esophagi, but reached much higher values of Cauchy stress, which are even higher than the rupture strength measured here. Yang et al. (2006a) also measured the stress-strain relationship of both layers at three different regions of the esophagus.

The high anisotropy in the muscle layer and the higher nonlinearity in the axial direction suggest that the fibers are strongly aligned along the axial direction, which applies also to the mucosa and the small intestine, but not in the same extent. To serve as a comparable alternative to naturally grown tissue, tissue engineered esophagi should show the same anisotropic, heterogenous and nonlinear biomechanical behavior. They should have a higher anisotropy in the muscle layer than in the mucosa, and a stronger nonlinearity along the axial direction than in the circumferential direction in both layers, like the ovine esophagi.

4.1.3 Rupture tests

The results for the uniaxial rupture tests are shown in Tables 3.8 and 3.9 and in Figure 3.7. The mean values of the rupture strength, in terms of the Cauchy stress σ, are

- 730 ± 307 kPa for the muscle in axial direction
- 630 ± 245 kPa for the muscle in circumferential direction
- 2556 ± 1004 kPa for the mucosa in axial direction
- 1537 ± 714 kPa for the mucosa in circumferential direction.

The ratio of axial to circumferential rupture strength was 1.66 in the mucosal layer and 1.16 in the muscle layer. The ratio of the rupture strength between the mucosa and the muscle was 3.5 in axial direction and 2.44 in circumferential direction.
The values of the rupture strength of the small intestine samples, 1014 kPa in axial direction and 273 kPa in circumferential direction, are shown in Figure 3.8.

Yang et al. (2006a) found for porcine esophagi, that the ratio of axial to circumferential rupture strength was on average 2.34 in the porcine mucosa and 1.25 in the porcine muscle. They found, that the ratio of the rupture strength between the mucosal layer and the muscle layer was 5.5 in axial direction and 3.0 in circumferential direction. The differences of the rupture strength ratios of porcine and ovine esophagi could be a result of the different thickness ratios between muscle and mucosa layers of the two species.

The large difference of the rupture strength between the mucosa and the muscle layer could be a result of the higher concentration of collagen fibers in the mucosa. A low concentration of collagen fibers in the muscle layer could also explain the higher anisotropy of the rupture strength in the mucosa. The very low rupture strength of the ovine small intestine in the circumferential direction compared to the axial direction could be a result of the anisotropic distribution of the collagen fibers. A future study on the rupture strength of tissue engineered esophagi should reveal similar values and an equally high heterogeneity in order to be a suitable substitution for naturally grown tissue.

4.1.4 Inflation tests

The results for the inflation tests of the esophagus are shown in Table 3.10 and in the Figs. 3.9 and 3.10.
All four series showed a high standard deviation, what made it difficult to interpret the results, but what was obvious was, that the esophagi showed a strong softening in circumferential direction during the series, which reached its maximum at a pre-stretch level of 30 %. With higher levels of pre-stretch the samples become stiffer. The axial stretch λ_z of the samples showed also a slight increase during the test with a much smaller standard deviation than λ_c, which additionally decreased strong with higher axial pre-stretch.
Table 3.11 and Figs. 3.11 and 3.12 show the results of the inflation tests of the small intestine with a circumferential stretch of nearly 50 % at 0 % pre-stretch and nearly 40 % at 10 % pre-stretch and an axial stretch of 6 and 12 % at 0 and 10 % pre-stretch respectively.

Yang et al. (2006b) tested the inflation behavior of the separated layers of porcine esophagi between 0 and 5 kPa and with axial pre-stretches of 0, 12.5 and 25 %. Their results show a nonlinear behavior of the layers with a more significant increase of the radius in the mucosal layer, and a stiffening with increasing pre-stretch. In contrast, Stavropoulou et al. (2009) found a higher increase of the radius in the muscle layer of rabbit esophagi between 0 and 1.4 kPa at axial stretch ratios of 1.2, 1.3, 1.4 and 1.5. Zeng et al. (2004) investigated the circumferential and axial stress-strain relation of inflated rat esophagi and found that the mucosa was stiffer than the muscle both in circumferential direction due to inflation and in axial direction due to elongation.

The strong softening in circumferential direction is possibly a result of the passive response of the muscle layer to occuring stresses, which stems from the low amount of collagen fibers and the non-active response of the muscle fibers (Liao et al., 2009) . A strong softening in circumferential direction at low pre-stretches and an axial stiffening with increasing axial pre-stretch of tissue engineered esophagi would reveal a similar passive response to extension-inflation like their naturally grown counterparts.

4.2 Error discussion

Systematic errors, which influenced the measurements, stem from the resolution of the load cells (0.03 % for the load cell of the tensile tests, 0.015 % for the bending load cell and 20 Pa for the pressure transducer), the stroke resolution of the fixing clamps (0.4 μm) and the resolution of the camera (795 pixel $\times$ 596 pixel).

4.3 Limitations

The results of these tests are subject to limitations, which have to be further investigated. These limitations are: For the uniaxial tests of the mucosa layer, most of the connective tissue of the submucosa had been removed. Since the submucosa consists mostly of collagen fibrils and is a important part of the mechanical resistance of the wall against deformation, it's removing can cause a change in the mechanical properties (Natali et al., 2009), (Yang et al., 2006a).
The layer specific tests are only uniaxial tests. Since uniaxial tests do not correspond to the *in vivo* state of the esophagus (Yang et al., 2006a), the results of the biaxial tests obtained by Georg Zeindlinger, MSc. as part of this project have also to be considered.
The results of the inflation tests have to be considered with high caution, because not all samples were tested with axial pre-stretches of 10, 20, 30 and 40 %. Some tests were started with 20 % and some did not reach 40 % pre-stretch. This had a strong influence on the statistics and is one cause of the high standard deviation, occuring in these tests.
Since the position of the samples along the esophagus were chosen randomly, changes in

the biomechanical behavior along the axial length of the esophagus were not considered. Storage of the small intestine sample in the freezer could have an effect on the measured behavior.

4.4 Perspectives

Future analysis of the collected data will include the determination of material parameters in the realm of hyperelastic continuum mechanics. The hyperelastic constitutive model by Holzapfel et al. (2000) or its extensions (Holzapfel et al., 2005), (Gasser et al., 2006), are appropriate to include the mechanical data presented herein. The model will be fitted to the uniaxial tensile and extension-inflation data, incorporating histological structure data, to obtain constitutive material parameters. This enables finite element simulations of the esophagus of, e.g., the act of swallowing or during extension following surgery.

Saxena et al. (2010) have shown, that it is possible to form a hollow tubular construct, consisting of a porous collagen scaffold draped around a endotracheal stent and seeded with esophageal epithelial cells. These experiments were successful in developing a rudimentary esophageal conduit with a constant thickness of 4 mm. Although these conduits show morphological and macroscopical density and ingrowth of the epithelial cells into the collagen scaffold, histologic investigations have revealed the fragility of the segments. Biaxial tensile tests of the used collagen scaffolds have revealed a stiffness which is much higher than that of the esophageal tissue. At the moment, the tissue engineered esophagi are not a suitable replacement of naturally grown esophagi. Future developments are necessary to obtain a more sophisticated mechanical behavior, closer to that of the natural esophageal tissue.

Bibliography

E. Brandenburger Technische Mechanik Teil 3: Festigkeitslehre. Script, Hochschule Karlsruhe, 2011.

D. C. Clark. Esophageal Atresia and Tracheoesophageal Fistula. *American Familiy Physician*, 59:910–916, 1999.

A. Faller *Der Körper des Menschen Einführung in Bau und Funktion*. Georg Thieme Verlag, Stuttgart, 2004.

K. Floyd and J. F. B. Morrison. The mechanical properties of oesophageal striated muscle in the cat and sheep. *J. Physiol.*, 248:717–724, 1974.

Y. C. Fung. What principle governs the stress distribution in living organisms? *Biomechanics in China, Japan, and USA*. Science Press., Beijing, 1–13, 1983.

Y. C. Fung. *Biomechanics: mechanical properties of living tissue*. 2nd ed. Springer-Verlag Inc., New York, 1993.

T. C. Gasser, R. W. Ogden, and G. A. Holzapfel. Hyperelastic modelling of arterial layers with distributed collagen fibre orientations. *J. R. Soc. Interface*, 3:15–35, 2006.

D. Geneviève, L. de Pontual, J. Amiel, S. Sarnacki and S. Lyonnet. An overview of isolated and syndromic oesophageal atresia. *Clinical Genetics*, 71:392–399, 2007.

H. Gregersen. *Biomechanics of the Gastrointestinal Tract*. Springer-Verlag Inc., London, 2003.

G. A. Holzapfel. *Nonlinear Solid Mechanics. A Continuum Approach for Engineering*. John Wiley & Sons, Chichester, 2000.

G. A. Holzapfel, T. C. Gasser, and R. W. Ogden. A new constitutive framework for arterial wall mechanics and a comparative study of material models. *Journal of Elasticity*, 61: 1–48, 2000.

G. A. Holzapfel, G. Sommer, T. C. Gasser, and P. Regitnig. Determination of layer-specific mechanical properties of human coronary arteries with nonatherosceloric intimal thickening and related constitutive modeling. *Am J Physiol Heart Circ Physiol*, 281:2048–2058, 2005.

J. D. Humphrey. *Cardiovascular Solid Mechanics: Cells, Tissues, and Organs*. Springer-Verlag Inc., New York, 2002.

D. Liao, J. Zhao, P. Kunwald and H. Gregersen. Tissue softening of guinea pig oesophagus tested by the tri-axial test machine. *Journal of Biomechanics*, 42:804–810, 2009.

K. Loeffler. *Anatomie und Physiologie der Haustiere*. Eugen Ulmer Verlag, Stuttgart, 1991.

I. Mann *Digestive track of sheep*
URL `http://ohioline.osu.edu/sc156/images/rb156_2.gif`

A. N. Natali, E. L. Carniel and H. Gregersen. Biomechanical behaviour of oesophageal tissues: Material and structural configuration, experimental data and constitutive analysis. *Medical Engineering & Physics*, 31:1056–1062, 2009.

A. K. Saxena, H. Baumgart, C. Komann, H. Ainoedhofer, P. Soltysiak, K. Kofler, M. E. Hoellwarth. Esophagus tissue engineering: in situ generation of rudimentary tubular vascularized esophageal conduit using the ovine model. *Journal of Pediatric Surgery*, 45:859–864, 2010.

C. A. J. Schulze-Bauer, P. Regitnig and G. A. Holzapfel. Mechanics of the human femoral adventitia including the high-pressure response. *Am. J. Physiol. Heart. Circ. Physiol.*, 282:2427-2440, 2002.

D. A. Scott. Esophageal Atresia/Tracheoesophageal Fistula Overview. *GeneReviews*, 2009.

D. P. Sokolis. Strain-energy function and three-dimensional stress distribution in esophageal biomechanics. *Journal of Biomechanics*, 43:2753–2764, 2010.

G. Sommer. Schichten-spezifisches mechanisches Verhalten menschlicher Koronararterien. Master's thesis, University of Technology, Graz, 2003.

G. Sommer, T. C. Gasser, P. Regitnig, M. Auer and G. A. Holzapfel. Dissection Properties of the Human Aortic Media: An Experimental Study. *J. Biomech. Eng.*, 130:021007-1-021007-12, 2008.

E. A. Stavropoulou, Y. F. Dafalias and D. P. Sokolis. Biomechanical and histological characteristics of passive esophagus: Experimental investigation and comparative constitutive modeling. *Journal of Biomechanics*, 42:2654–2663, 2009.

R. N. Vaishnav and J. Vossoughi. Estimation of residual strains in aortic segments. *Biomedical Engineering II, Recent Developments, Vol. 2*. Pergamon Press., Oxford, 330–333, 1983.

Wikipedia entry: In vivo, August 18, 2011
URL `http://en.wikipedia.org/wiki/In_vivo`

W. Yang, T. C. Fung, K. S. Chian and C. K. Chong. Directional, Regional, and Layer Variations of Mechanical Properties of Esophageal Tissue and its Interpretation Using a Structure-Based Constitutive Model. *J. Biomech. Eng.*, 128:409–418, 2006.

W. Yang, T. C. Fung, K. S. Chian and C. K. Chong. 3D Mechanical Properties of the Layered Esophagus: Experiment and Constitutive Model. *J. Biomech. Eng.*, 128:899–908, 2006.

W. Yang, T. C. Fung, K. S. Chian and C. K. Chong. Viscoelasticity of Esophageal Tissue and Application of a QLV Model. *J. Biomech. Eng.*, 128:909–916, 2006.

J. Yang, J. Zhao, D. Liao and H. Gregersen. Biomechanical properties of the layered oesophagus and its remodelling in experimental type-1 diabetes. *Journal of Biomechanics*, 39:894–904, 2006.

A. Yavari *Quasi-static loading*
URL `http://imechanica.org/node/8437`

S. Zachow *Viskoelastiztät*
URL `http://public.tfh-berlin.de/~stevie/mod+sim/node42.html`

Y-J. Zeng, J. Yang, J-B. Zhao, D-H. Liao, E-P. Zhang, H. Gregersen, X-H. Xu, H. Xu, C-Q. Xu. Morphologic and biomechanical changes of rat oesophagus in experimental diabetes. *World Journal of Gastroenterology*, 10:2519–2523, 2004.

Deutsche Fassung:
Beschluss der Curricula-Kommission für Bachelor-, Master- und Diplomstudien vom 10.11.2008
Genehmigung des Senates am 1.12.2008

EIDESSTATTLICHE ERKLÄRUNG

Ich erkläre an Eides statt, dass ich die vorliegende Arbeit selbstständig verfasst, andere als die angegebenen Quellen/Hilfsmittel nicht benutzt, und die den benutzten Quellen wörtlich und inhaltlich entnommene Stellen als solche kenntlich gemacht habe.

Graz, am ……. ……..
(Unterschrift)

Englische Fassung:

STATUTORY DECLARATION

I declare that I have authored this thesis independently, that I have not used other than the declared sources / resources, and that I have explicitly marked all material which has been quoted either literally or by content from the used sources.

……. ……..
date (signature)